A comparison between different methods to determine moisture transport properties of cementitious materials

Nilsson, Lars-Olof

2013

LUND INSTITUTE OF TECHNOLOGY
LUND UNIVERSITY

Division of Building Materials

A comparison between different methods to determine moisture transport properties of cementitious materials

Lars-Olof Nilsson

Funded by Formas, the Swedish Research Council for Environment, Agricultural Sciences and Spatial Planning

Report TVBM-3168 Lund 2013

ISRN LUTVDG/TVBM--10/3168--SE(1-47)
ISSN 0348-7911 TVBM

Lund University, Faculty of Engineering
Laboratory of Building Materials
Box 118
SE-221 00 Lund, Sweden

Telephone: 46-46-2227415
Telefax: 46-46-2224427
www.byggnadsmaterial.lth.se

Preface

In the project ”Crack-Free-Con - Nordic coordination for a sustainable construction by novel shrinkage modelling and user friendly Expert System”, funded by Formas, there was a need to select a method for quantifying the moisture transport properties of any new concrete. This report describes a separate experimental study to compare different methods to make that kind of measurements.

All preparation of specimens and all measurements have been performed by laboratory engineer Bo Johansson in an excellent way.

Holcim Ltd., a partner to Lund University within the cement research network NanoCem, nanocem.org, has supplied the Portland cement binder for the specimens.

The experimental study has been selected as the Partner Project of Lund University 2009-2012 within NanoCem.

Summary

A number of methods for measuring moisture transport properties of cementitious materials were compared in a series of experiments. Two OPC-mortars with two water-binder-ratios were wet cured for six months and used to produce specimens as discs with different thicknesses and diameters.

The cup methods were easy to use, reliable and fairly rapid but need a stable, surrounding, CO_2-free climate, however. Evaluating the fundamental potential PSI eliminates the derivation that adds to the uncertainty.

Steady-state moisture distribution measurements are very time-consuming and the RH-profiling is a delicate matter. Moisture contents are scattering.

Sorption experiments are very easy to perform but difficult to evaluate, because of the peculiar moisture-dependency of the diffusivity D_w and the difficulties to estimate the equilibrium conditions. Initial uniform conditions are difficult to obtain for low w/c-materials, except to initial self-desiccation. Sorption experiments in small steps are uncertain; the initial and final conditions are difficult to define properly.

Sammanfattning

Ett antal metoder för att bestämma fukttransportegenskaper hos cementbaserade material har jämförts i en serie experiment. Två Portlandcementbruk med två vattencementtal härdades i vatten under sex månader och användes för att tillverka provkroppar med olika tjocklek och diameter.

Koppmetoden var enkel att använda, tillförlitlig och relativt snabb, men kräver ett stabilt, CO_2-fritt omgivande klimat. Utvärdering av fundamentalpotentialen PSI är enkel och eliminerar derivering som ökar osäkerheten.

Bestämning av stationär fuktfördelning och fuktflöde är mycket tidsödande och mätning av RF-profilen är svårt. Att mäta fuktkvotsprofiler för betong och bruk ger stor spridning och därmed osäkra resultat.

Sorptionsexperiment är mycket enkla att genomföra men svåra att utvärdera, dels därför att sluttillståndet är osäkert och dels därför att diffusiviteten D_w har ett märkligt fuktberoende. Konstant startfuktfördelning är svår att uppnå annat än för ren självuttorkning. Sorptionsexperiment i små steg är osäkra; start- och sluttillstånden är svåra att uppnå.

List of Contents

1 Introduction 1
- 1.1 Background of the over-all project 1
- 1.2 Over-all objectives 1
- 1.3 Over-all project plan 2
- 1.4 Objectives of the experimental study 2

2 Test methods for moisture transport properties 3
- 2.1 Mathematical models for moisture transport 3
- 2.2 Steady-state test methods for moisture transport 5
- 2.3 Non-steady-state test methods for moisture transport 8
  - 2.3.1 Methods based on moisture profile measurements 8
  - 2.3.2 Methods based on capillary suction tests 8
  - 2.3.3 Sorption methods 8

3 Materials and specimens 11
- 3.1 Materials 11
- 3.2 Specimens 12

4 The Cup method 14
- 4.1 Experimental set-up 14
- 4.2 Weight changes, mortar I 15
- 4.3 Weight changes, mortar II 18
- 4.4 Evaluation of steady-state fluxes, average δ and PSI 22
- 4.5 Evaluation of the moisture dependency of δ(RH) 25
- 4.6 Conclusions on cup methods 27

5 Steady-state moisture profile method 28
- 5.1 Experimental set-up 28
- 5.2 Flux measurements 28
- 5.3 Moisture profile measurements 29
  - 5.3.1 Moisture content profiles 29
  - 5.3.2 RH-profiles 30

6 Non steady-state moisture profile method 35
- 6.1 Experimental set-up 35
- 6.2 Weight measurements 35
- 6.3 Moisture profile measurements 36
  - 6.3.1 Moisture content profiles 36
  - 6.3.2 RH-profiles 37
- 6.4 Evaluation 38

7 Non steady-state sorption method 40
- 7.1 Experiments 40
- 7.2 2L=75 mm 40
- 7.3 2L=15 and 45 mm 43

8 Conclusions 45

References 46

1 Introduction

In the project ”Crack-Free-Con - Nordic coordination for a sustainable construction by novel shrinkage modelling and user friendly Expert System”, funded by Formas, there was a need to select a method for quantifying the moisture transport properties of any new concrete. This report describes a separate experimental study to compare different methods to make that kind of measurements.

The background of the project, as described in the original research program, is briefly repeated here, together with the objectives.

1.1 Background of the over-all project

In concrete structures cracks cannot be tolerated. Besides impairing the durability or function, cracking may also be aesthetically unacceptable. Costly repairs of cracked concrete are common and, in some cases, it is even necessary to demolish severely cracked structures at an age much lower than lifetime. Hence, it is a significant task developing methods to control cracking.

Today, computer based Expert Systems exist for calculating thermally induced cracking risks and for suggesting proper thermal crack avoiding measures. Thus, with Nordic concepts (code regulations, computer programs, laboratory test etc), e. g. developed within IPACS and Nor-IPACS projects, occurrence of thermal cracking indeed has been reduced in practice.

However, it is well known that shrinkage due to moisture changes also is one of the main mechanisms causing concrete cracking. Therefore, it is surprising that no reliable theoretical model or computer program exists that considers the effect of shrinkage on cracking.

Furthermore, shrinkage formulas in concrete Codes are not valid for modern concrete qualities and binders and the models very briefly or not at all consider the primary phenomena - the simultaneous autogenous and drying moisture changes in the material.

1.2 Over-all objectives

The objective after finalization of the project is to secure construction of crack free sustainable concrete structures. To achieve this, the project objectives are to:

- Establish a novel shrinkage model based on fundamental knowledge of moisture state, which implies a test setup for accurate laboratory documentation.
- To include the reliable shrinkage modelling into the present Expert systems (mentioned above) of estimation of restraint stresses and cracking risks, cf. figure 1.

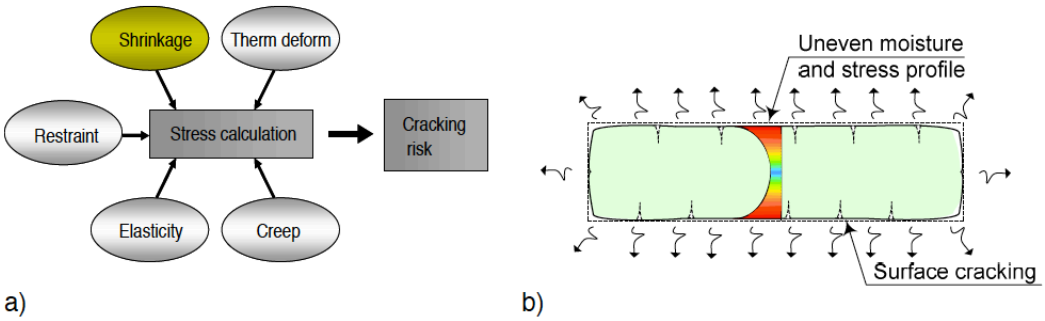

Figure 1 a) Expert system for crack risk estimation – components required for assessing shrinkage and thermally induced stresses.

b) The dilemma of drying shrinkage testing and modelling is the uneven humidity conditions resulting in eigenstresses, potential to surface cracking and size effects

1.3 Over-all project plan

In accordance with the objectives, the project plan is divided into three parts:

1. Establishment of a test methodology for correct analysis of autogenous and drying shrinkage
2. Modelling of moisture and shrinkage in test specimen as well as structural humidity changes and shrinkage based on (1)
3. Data on humidity and shrinkage for common concrete mixes
4. Integrating of model in existing systems for crack estimation, pilot crack estimations
5. Computer based tool for crack risk estimations, implementation in full scale use.

This experimental study is meant to find a method for quantifying input data for the modelling in point (2) and quantify the data in point (3).

1.4 Objectives of the experimental study

The objectives of the separate experimental study were the assessment of alternative methods to measure macroscopic moisture transport properties of cementitious materials and the clarification of the moisture dependency of various moisture transport coefficients. Nano-macro linkages are searched for as explanations.

2 Test methods for moisture transport properties

In the research program to develop new methods for evaluating shrinkage measurements, a model for drying is required. An essential part of such a model is the description of moisture transport properties. In this study several different techniques were used to make direct or indirect measurements of these properties and to compare and verify them against drying experiments.

Presently, several methods are used to measure moisture transport properties and numerous mathematical expressions for flux of moisture are used in models for moisture changes and variations. The results are frequently not well understood and do not always coincide. Different methods give different results! This must be clarified.

2.1 Mathematical models for moisture transport

Traditionally, moisture transport in porous materials is mathematically described with one or two terms (in rare cases three). Different transport potentials are used. If only one term is to be used, you can choose between these:

a. pore humidity H [-]
b. vapour content v [kg/m^3]
c. pore water pressure P_w [Pa]
d. partial vapour pressure p_v [Pa]
e. chemical potential μ [-]
f. moisture content w [kg/m^3]
g. degree of saturation S [-]
h. capillary degree of saturation S_{cap} [-]

The first five are physically motivated. The are all possible to translate into each other. Consequently, anyone can be chosen, at least at constant temperature.

The translation between the five states of moisture a-e are

$$H = \frac{v}{v_m} = \frac{p_v}{p_{v,m}} \quad (1)$$

$$p_v = v \cdot \frac{RT}{M} \quad (2)$$

$$P_w = p_{v,m} + \frac{RT\rho}{M} \ln(H) \quad (3)$$

$$\mu(T, P, p_v) = \frac{RT}{M} \ln(H) \quad (4)$$

To translate the moisture transport potentials a-e into one of the last three f-h, the sorption isotherm w(H) is required.

Frequently, attempts are made to describe moisture transport with mathematical expressions that are motivated by the transport mechanisms, i.e. vapour content or vapour pressure for vapour transport and pore water pressure for liquid water transport. Then two terms are added, one supposed to describe vapour flow and one describing liquid flow. There are at least two reasons why this approach does not work:

1. There are more mechanisms than vapour and liquid flow in cementitious (and other) materials, such as adsorbed water flow.
2. Only the total flux can be measured; vapour, adsorbed and liquid flow cannot be separated.

The reason for using two terms in a moisture transport model is another one. As long as there is no temperature gradient, any of the transport potentials a-h is usable, since they can be recalculated into each other. That means that only one term is required. With moisture flow along a temperature gradient this translation depends on the gradient and vapour, adsorbed and liquid flow may very well occur in different directions. Consequently, more than one transport potential is required.

Examples of mathematical descriptions of the flux *J* of moisture are given in equations (5)-(11).

$$J_v = -\delta_v \frac{\partial v}{\partial x} \tag{5}$$

$$J_l = -\frac{k_P}{\eta}\frac{\partial P_w}{\partial x} \tag{6}$$

$$J = -\delta_{tot}\frac{\partial v}{\partial x} \tag{7}$$

$$J = \frac{\Psi}{d} \tag{8}$$

$$J = -D_w \frac{\partial w}{\partial x} \tag{9}$$

$$J = -k_{RH} \frac{\partial \varphi}{\partial x} \tag{10}$$

$$J = -\delta_{vT} \frac{\partial v}{\partial x} - D_{wT} \frac{\partial w}{\partial x} = -\delta'_{vT} \frac{\partial v}{\partial x} - D_T \frac{\partial T}{\partial x} \tag{11}$$

The last equation (11) is an example of two ways to use two terms for moisture transport along a temperature gradient.

Equation (8) describes the "fundamental potential" Ψ as a direct way to express the flux of moisture. $\Psi(H_1, H_2)$ is the flux of moisture through a slice of a material with a thickness d, when the humidity on the two opposite sides of the slice is H_1 and H_2, respectively. Ψ has some numerical advantages in computer modelling.

A "moisture transport property" is one of the coefficients in these equations, e.g. that property is always related to a moisture transport model.

It should be pointed out that the moisture transport properties, the coefficients, almost laways are significantly moisture dependent!

2.2 Steady-state test methods for moisture transport

The steady-state methods for quantifying moisture transport properties are characterized by two things:

a. one of the moisture flux equations with one term is selected
b. the steady-state moisture flux *J* is measured

The principle is simple: perform an experiment with a specimen with a certain thickness, expose it to constant but different climatic conditions on the two opposite surfaces and wait for the flux to be constant in time. Evaluate the moisture transport coefficient from the chosen equation. Use a series of climatic conditions to quantify the moisture dependency of the transport coefficient.

The most common steady-state method for moisture transport properties is the so-called cup method. A disc of the material is placed as a lid on a "cup", of glass or metal. The cup contains a saturated salt solution or a drying agent to control the humidity inside the cup. The cup is then placed in a climate box or a climate room to control the climate at the other side of the disc. The weight of the cup, including the disc and the sealing system, is regularly determined; the weight changes are easy to translate into a flux out of or into the cup. When it is constant in time, steady-state conditions have been reached.

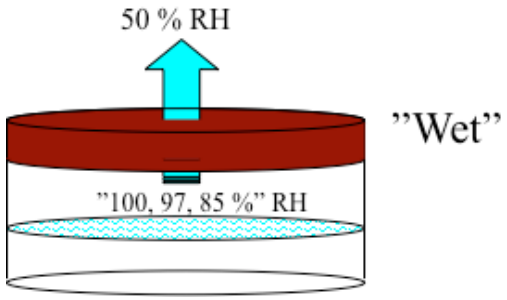

Fig. 2 A typical "wet cup" with more humid conditions inside the cup than outside it.

The moisture transport coefficient, e.g. δ_{tot} in equation (7), is then evaluated from the flux equation, cf. equation (12)

$$J = -\delta \frac{\partial v}{\partial x} = \delta \cdot v_s \frac{\Delta H}{\Delta x}$$
$$\delta = \frac{J \cdot \Delta x}{\Delta H \cdot v_s} \tag{12}$$

To use the correct humidity gradient over the disc of the material, the humidity conditions to be inserted into the selected equation should be the conditions at the very surface of the disc. Since a saturated salt solution controls the humidity just above the liquid surface of the solution that means that correction has to be made for the resistance to moisture flow of the air gap between the surface of the solution and the bottom surface of the disc.

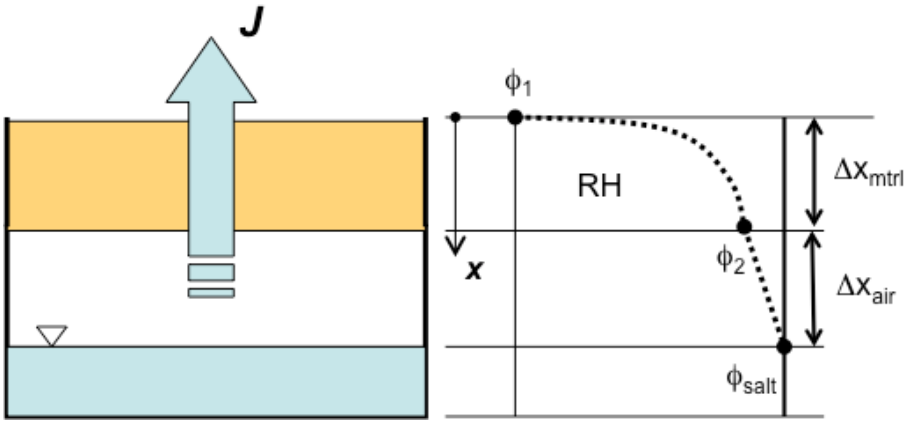

Fig. 3 The correction of the RH at the bottom surface of the disc because of the resistance to moisture flow of the air gap.

RH ϕ_2 at the bottom surface can be calculated from

$$J = D_v \frac{\Delta v_{air}}{\Delta x_{air}} = D_v \frac{\Delta \phi_{air} \cdot v_s}{\Delta x_{air}} = D_v \frac{(\phi_{salt} - \phi_2) \cdot v_s}{\Delta x_{air}} \quad which\ gives$$
$$\phi_2 = \phi_{salt} - \frac{J \cdot \Delta x_{air}}{D_v \cdot v_s} = \phi_{salt} - \Delta \phi_{air} \tag{13}$$

where D_v=25·10^{-6} m^2/s is the moisture transport coefficient of water vapour in air.

To be able to measure properties for humidity levels as close to 100 % RH as possible, the drop in RH because of the resistance of the air gap can be avoided by using a so-called "inverted cup" or "upside-down cup", with water in direct contact with the surface of disc inside the cup, cf. figure 4.

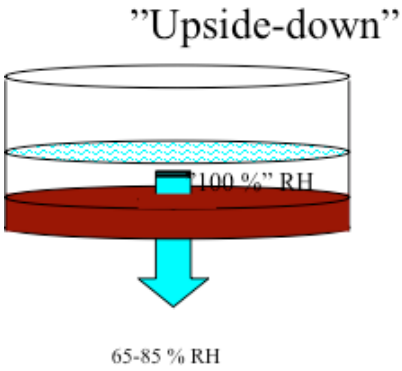

Fig. 4 An “upside-down cup” or “inverted cup” with water in direct contact with the surface of the disc.

The cup method has been used by numerous researchers, also for cementitious materials, and is standardized internationally.

Another steady-state method is using a thicker specimen to be able to measure the moisture profile once steady-state flux has been achieved. The moisture profile can be measured by slicing the specimen or by inserting humidity probes in holes perpendicular to the moisture flux direction. From the moisture profile at steady-state conditions the moisture gradient is directly evaluated and inserted into the selected moisture flux equation.

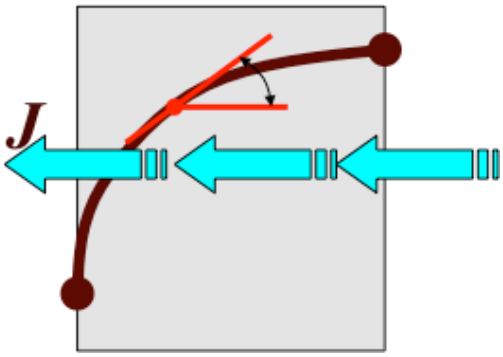

Fig. 5 The principle of the steady-state method to quantify the full moisture dependency of a moisture transport coefficient from one specimen by measuring the moisture profile after steady-state flux has been reached.

The advantage with the latter method is that the full moisture dependency can be determined from one and the same specimen. The draw-back is, of course, the extremely long time required to reach steady-state moisture flux for a thick specimen. A detailed study with this method was done on aerated concrete by van der Kooi (1971). An extensive study of moisture transport coefficients for mature concrete, mortar and paste was done with this method by Hedenblad (1993).

2.3 Non-steady-state test methods for moisture transport

The non-steady-state methods for quantifying moisture transport properties are utilizing measurements of changes in moisture conditions or moisture contents with time.

2.3.1 Methods based on moisture profile measurements

In the most sophisticated non-steady state methods moisture profiles are determined, destructively or non-destructively, with various methods. From the differences between the moisture profiles at different times fluxes and gradients are determined at different moisture levels and from those the moisture dependency of the transport coefficient is evaluated.

2.3.2 Methods based on capillary suction tests

A simple capillary suction test, starting at different initial moisture contents, can also be used as a non-steady state method for determining the moisture dependency of the moisture transport coefficient. The experiments are simple but the conditioning to constant initial moisture content is very difficult, especially when trying to avoid the effects of hysteresis close to the surfaces, and time-consuming.

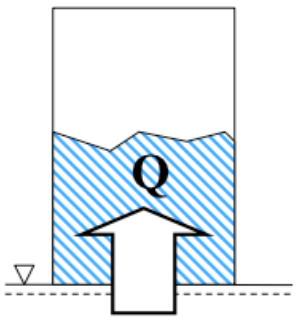

$$\mathbf{Q} = \mathrm{A}\sqrt{\mathrm{t}}$$

Fig. 6 The simple sorptivity test that can be used to evaluate the moisture dependency of the moisture diffusivity by starting from a series of initial moisture contents

It is easy to evaluate the sorptivity from the capillary suction tests but it is a very complicated evaluation to derive the diffusivity D_w. The first to do it was Janz (2000), for natural stone. Johansson (2003) did it for a few materials, including a cement mortar.

2.3.3 Sorption methods

The sorption methods are based on a special version of the mass-balance equation for moisture, using the moisture transport equation (9):

$$\frac{\partial w}{\partial t} = -\frac{\partial J}{\partial x} = \left[Eq.(9) \right] = \frac{\partial}{\partial x} D_w \frac{\partial w}{\partial x} \qquad (14)$$

The changes of average moisture content w can easily be translated into weight changes. In this way a mathematical solution to the mass-balance equation can be compared to the weight changes with time.

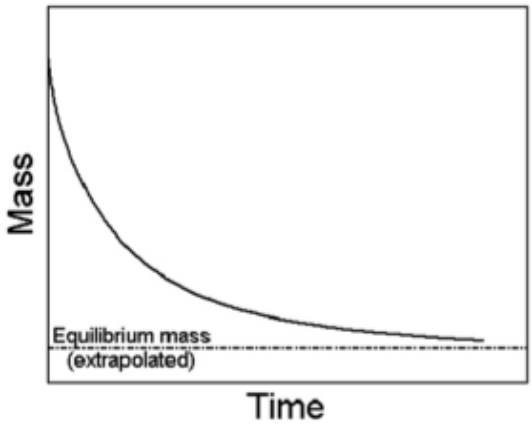

Fig. 7 The experimental results from a sorption method where the drying of a specimen is followed by determining the weight changes with time.

The sorption method starts with conditioning a specimen to initial conditions that are equal at all depths. Then the specimen is placed in another climate, more or less humid than the initial conditions, and the wetting or drying of the specimen are followed by determining the weight changes. The weight changes can hardly ever be followed to equilibrium with the surroundings since that, theoretically, requires infinite time. Consequently, the equilibrium conditions must be estimated or quantified with a parallel experiment.

The analytical solution to the mass-balance equation (12) is shown in figure 8

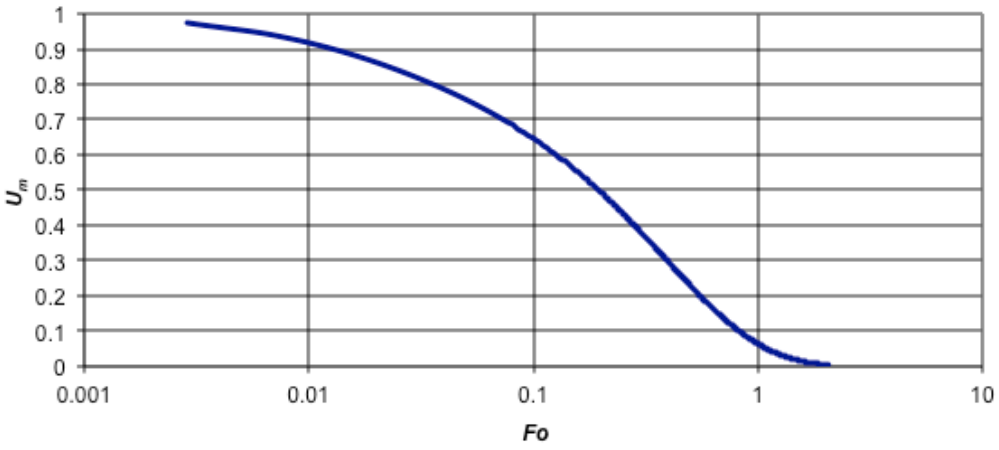

Fig. 8 The analytical solution to the mass-balance equation for a step-change, where a 1D-specimen changes its, initially constant, moisture content in a constant climate, with no surface resistances.

In figure 8 the two parameters are the average drying potential U_m and the Fourier number F_0

$$U_m = \frac{\bar{w} - w_\infty}{w_0 - w_\infty} \tag{15}$$

$$F_0 = \frac{D_w \cdot t}{L^2} \tag{16}$$

where $\bar{w}$ is the average moisture content, w_0 is the initial moisture content, w_∞ is the equilibrium moisture content, D_w is the moisture diffusivity, t is the time and L is the characteristic thickness of the specimen (L = half the thickness of a disc with 1D two-sided drying).

The analytical solution in figure 8 requires the diffusivity D_w to be a constant. This is rarely true, which means that the step-changes must be within small humidity intervals where the diffusivity is assumed constant. If not, the measured weight changes should be compared with a numerical solution to the mass balance equation.

The solution in figure 8 is based another assumption, the surface resistance to moisture flow being zero or negligible. For thin, wet specimens of materials with a large moisture transport capacity this could affect the sorption results so the solution in figure 8 is no longer correct. Then, the size-effect according to equation (16) does not fit anymore.

Many researchers have used the sorption method. Nilsson (1980) and Baroghel-Bouny (2007) are two of them that applied the method to cement-based materials. Wadsö (1989) described traditional applications and some new ideas for the method.

3 Materials and specimens

3.1 Materials

Two mortars were used for the specimens. The mortars were mixed with fine-grained sand and Holcim OPC (CEM I 42.5N) as binder. The cement composition is shown in Table I, Olsson et al (2012).

Table I Chemical analysis of the OPC-binder

Chemical Analysis XRF g/100g		Mineralogical Composition XRD/Rietveld analysis g/100g	
SiO_2	19.88	Alite	66.66
Al_2O_3	4.47	Belite	8.42
Fe_2O_3	2.96	Aluminate	6.17
CaO	63.49	Ferrite	9.60
MgO	1.77	Arcanite	1.60
K_2O	0.858	Free Lime	0.06
Na_2O	0.169	Portlandite	0.47
TiO_2	0.318	Periclase	0.49
Mn_2O_3	0.046	Gypsum	1.17
P_2O_5	0.219	Hemihydrate	2.18
SrO	0.049	Calcite	3.11
Cl	0.028	Anhydrite	0.10
F	<0.1		
ZnO	0.015		
Cr_2O_3	0.012		
SO_3	2.96		

Two water-binder ratios were used: w/c=0.38 & 0.53. The mix composition is shown in Table II, Olsson et al (2012).

Table II Mix composition of mortars, kg/m^3

Mortar	I	II
w/c	0.38	0.53
OPC	516	436
Water	196	231
Normsand	1548	1525
Plasticizer	1.18	-

The air contents of the mortar mixes were determined to 6.4 and 6.1 %, respectively.

The mortars were cast in large blocks and demoulded after one day of sealed curing. They were then cured in water for six months. A week after casting, 50 and 100 mm cylinders were drilled horizontally from the blocks and put

back in the holes in the blocks for further wet curing, to limit the leaching of alkalis during water curing.

The same mortars are being used in NanoCem's Core Project 8 that studies non-saturated transport of ions; diffusion and convection at different degrees of saturation.

3.2 Specimens

Two months after casting the cylinders were sliced into discs with thicknesses 15 mm and 45 mm (only 100 mm cores) and then put back into the water-filled holes for curing.

From these discs specimens for the moisture transport measurements were prepared after the six months of water curing. First the weight, diameter and thickness of each disc were measured.

Specimens with a diameter of 100 mm and thickness 15 mm were marked Ca to be put as lids on glass cups for the cup method. 21 discs were used for each of the two mortars. The edges of the discs were sealed with a rubber-bitumen-aluminium tape before put on top of the glass cups.

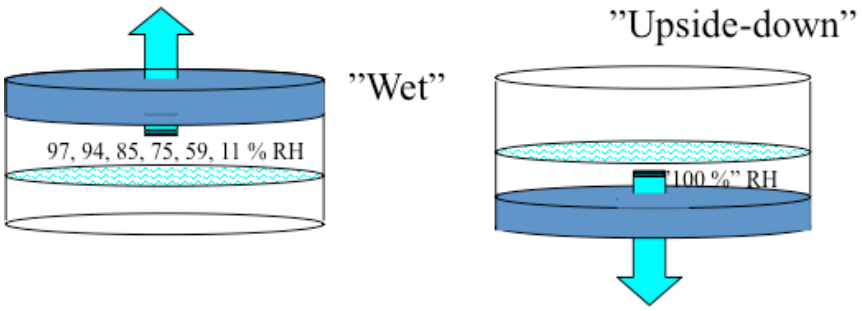

Fig. 9 15 mm thick discs with a diameter of 100 mm used as lids on glass cups in the cup method.

Specimens with a diameter of 50 mm and thickness 15 and 45 mm were marked Cb to be used for two-sided drying with the sorption method. The edges of these discs were also sealed with a rubber-bitumen-aluminium tape to ensure 1D moisture transport during drying.

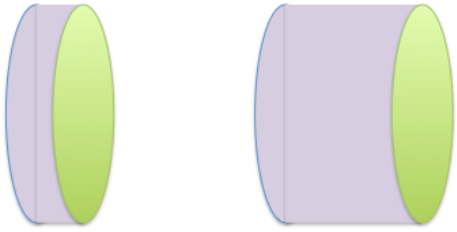

Fig. 10 15 and 45 mm thick discs with a diameter of 50 mm and edge sealed to be used in 1D-drying in sorption methods.

Six 15 mm and six 45 mm specimens were prepared for each mortar.

Specimens with a diameter of 50 mm and thickness 15 and 45 mm were marked Cc to be used for capillary suction tests.

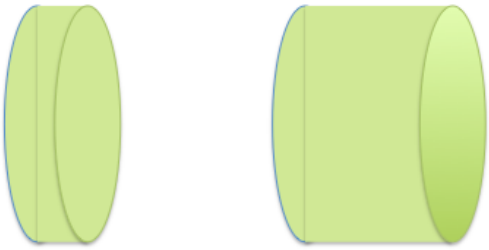

Fig. 11 15 and 45 mm thick discs with a diameter of 50 mm planned to be used in capillary suction tests.

Specimens with five discs with a thickness of 15 mm and a diameter of 50 mm were marked Cd, to be used for 1D drying and steady-state tests, cf. figure 12. One set of rolls was prepared with the two mortars.

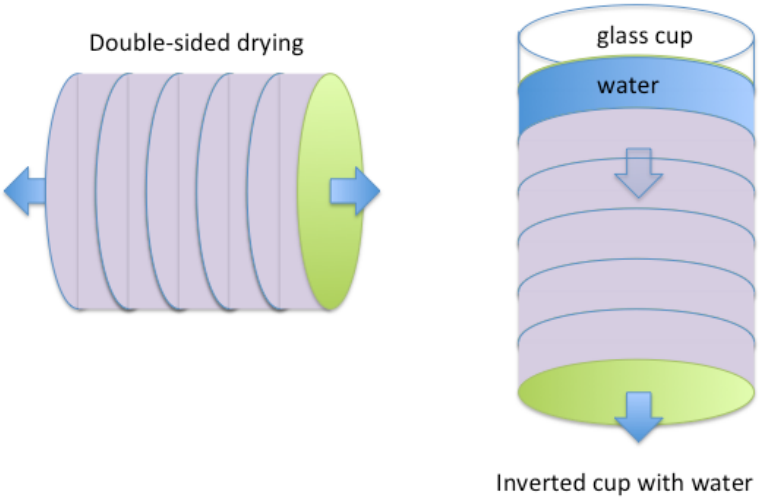

Fig. 12 "Rolls" of five 15 mm thick discs with a diameter of 50 mm and edge sealed to be used in 1D-drying non-steady state method (left) and a steady-state method (right).

A thin cloth of cotton was placed between the discs to ensure a good "moisture contact" between the discs. The circumference of these "rolls" was also sealed with a rubber-bitumen-aluminium tape to ensure 1D moisture transport during drying and steady-state moisture flow.

4 The Cup method

4.1 Experimental set-up

On top of glass cups 15 mm mortar discs with a diameter of 100 mm were mounted as lids and sealed with a rubber-bitumen-aluminium tape that covered the joint between the edge-sealed disc and the glass cup. The glass cups were filled with some 20 mm saturated salt solutions, giving 11 (LiCl), 59 (NaBr), 75 (NaCl), 85 (KCl), 95 KNO_3), 97 (K_2SO_4) % RH. The distance between the surface of the solution and the bottom surface of the disc was measured for each cup. "Inverted cups" were prepared with water, giving 100 % RH, and turned upside-down.

All the cups were placed on a plastic net in sealed climate boxes with a saturated salt solution (MgCl), giving 33 % RH. The plastic boxes had a heavy glass sheet as a lid and a rubber tube inbetween to seal between the box and the glass lid. The boxes also contained a cup with a CO_2-absorbent. The boxes were equipped with fans to circulate the air in the boxes and an RH-probe in each box.

One of the climate boxes with cups is shown in figure 13.

Fig. 13 One of the climate boxes with a glass lid containing nine cups, three of which inverted. The fan is visible to the left and the CO_2-absorbent beneath it.

The weights of the cups were determined regularly and each time the RH in the boxes was read, noted and translated an RH by use of a calibration curve, one for each RH-probe.

4.2 Weight changes, mortar I

The weight changes were determined for a period of, altogether, 244 days. The weight changes of all cups are shown in figures 14-20 for mortar I and in figures 21-26 for mortar II.

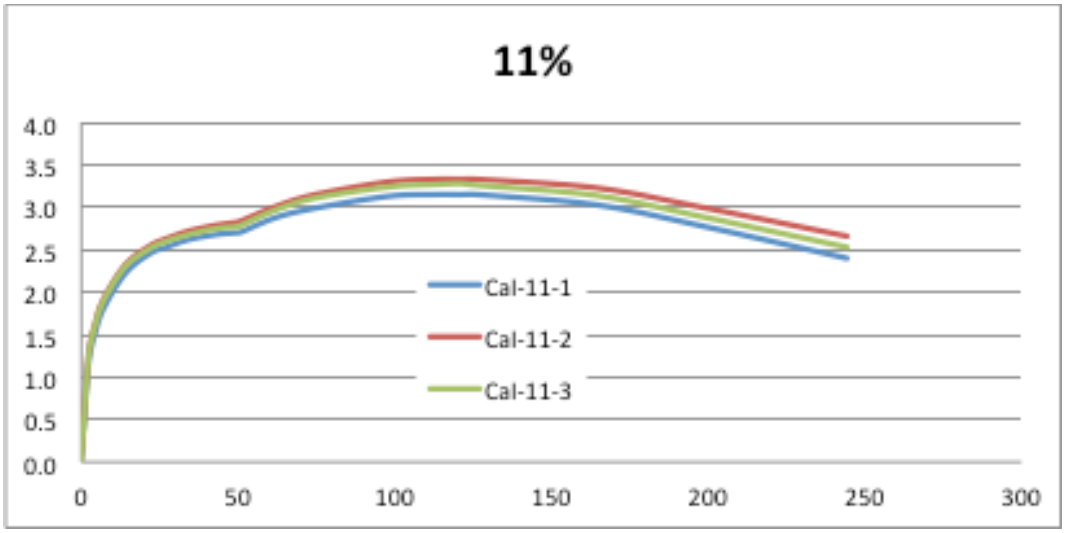

Fig. 14 Weight losses of the three cups with 11 % RH and discs CaI from mortar I.

The cups with 11 % RH inside the cups and 33 % RH outside the cups, in the box, loose weight at the beginning since the mortar discs are wet. Moisture from the discs dries out into the climate box but also into the cup and condenses in the "dry", saturated LiCl-solution. First after more than four months the cups start to gain weight and the direction of moisture flow is into the cups, from 33 % RH in the box into the 11 % RH in the cups.

More than six months are required to reach a steady-state flux through the discs.

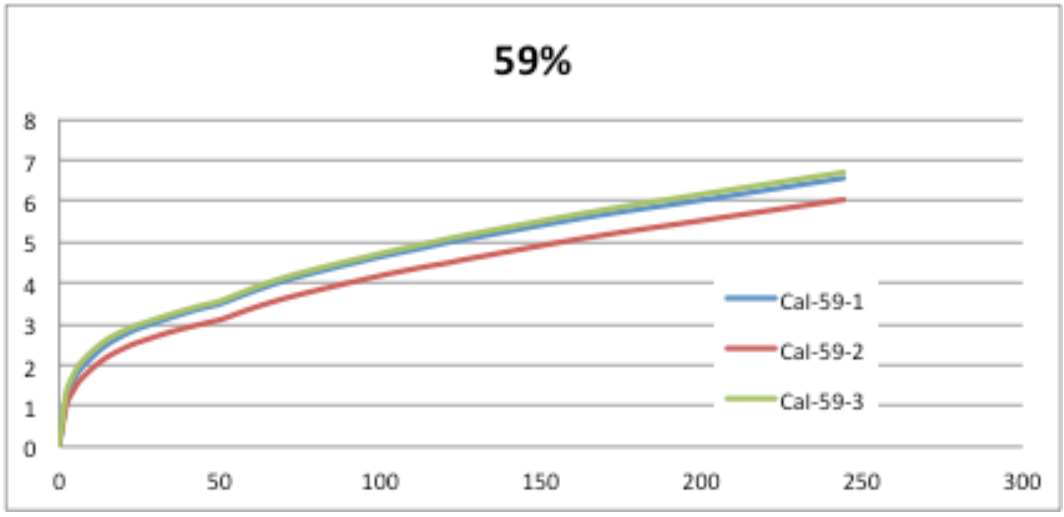

Fig. 15 Weight losses of the three cups with 59 % RH and discs CaI from mortar I.

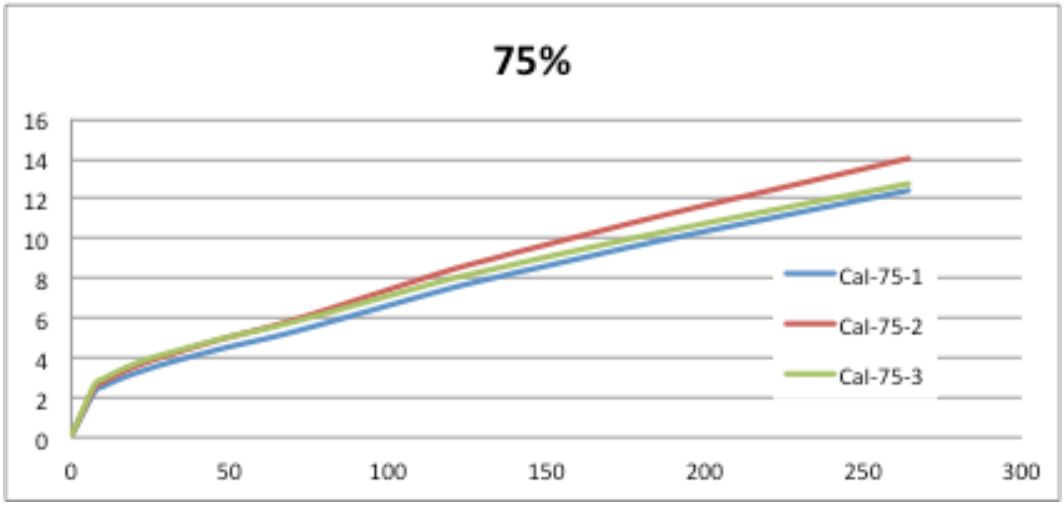

Fig. 16 Weight losses of the three cups with 75 % RH and discs CaI from mortar I.

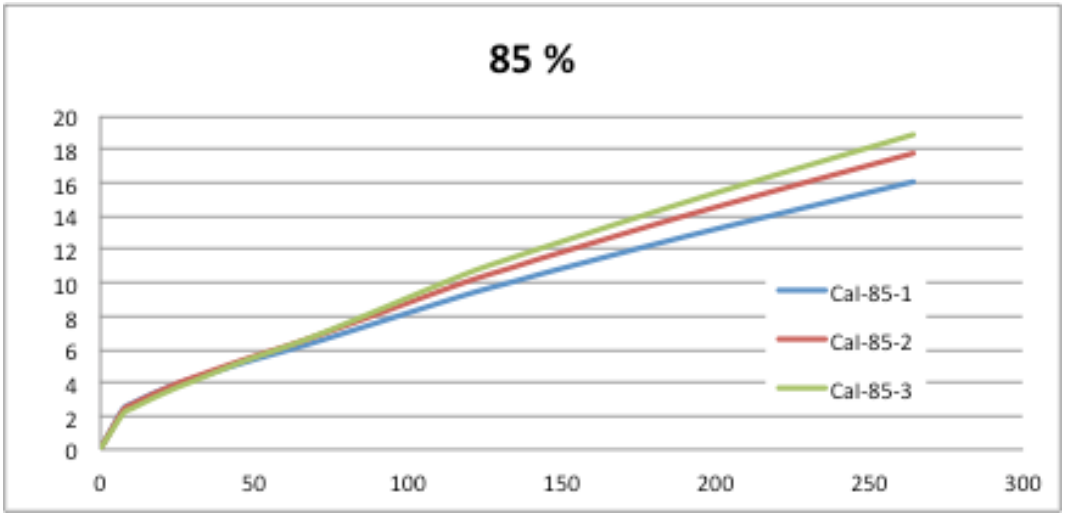

Fig. 17 Weight losses of the three cups with 85 % RH and discs CaI from mortar I.

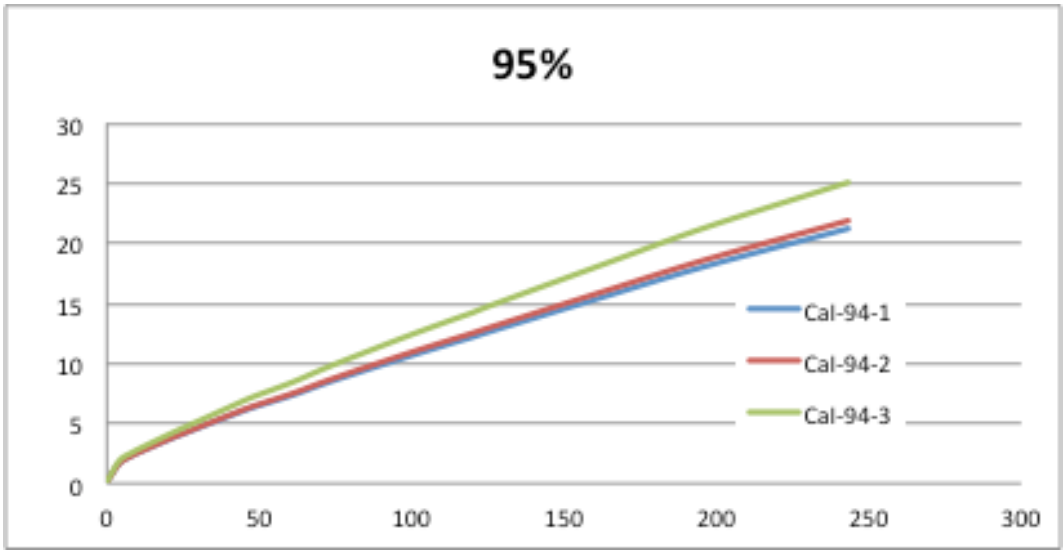

Fig. 18 Weight losses of the three cups with 85 % RH and discs CaI from mortar I.

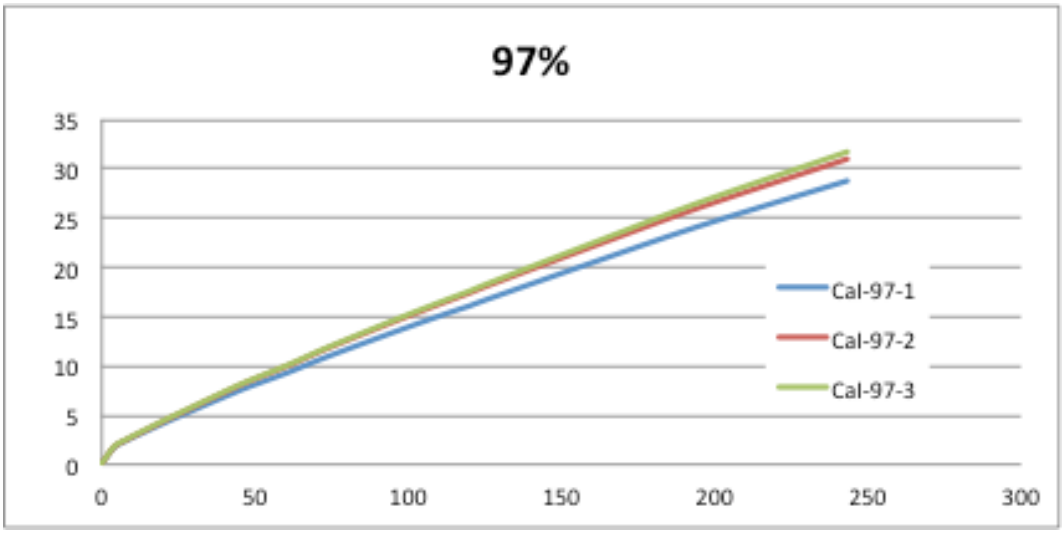

Fig. 19 Weight losses of the three cups with 97 % RH and discs CaI from mortar I.

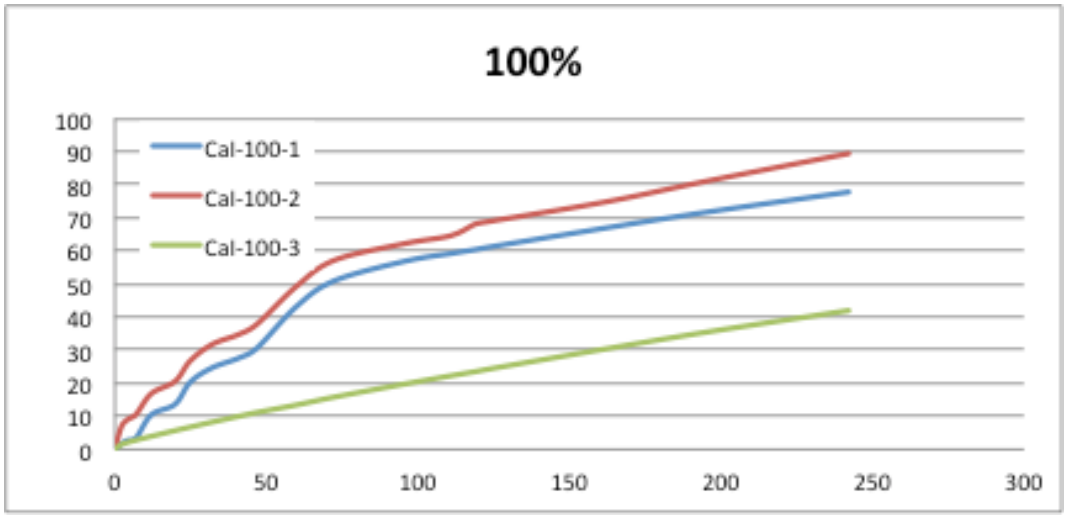

Fig. 20 Weight losses of the three "inverted cups" with 100 % RH and discs CaI from mortar I.

There were obviously leakages in two of the inverted cups, with direct contact between the discs and water, during the first two months. The third cup reached steady-state flux fairly quick.

4.3 Weight changes, mortar II

The weight changes of all cups with mortar II are shown in the same way in figures 21-27.

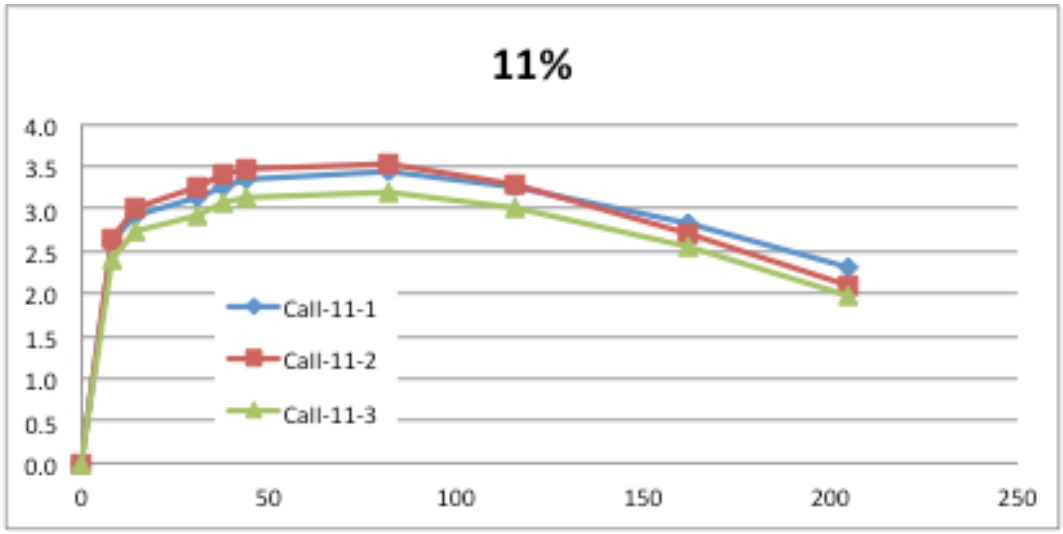

Fig. 21 Weight losses of the three cups with 11 % RH and discs CaII from mortar II.

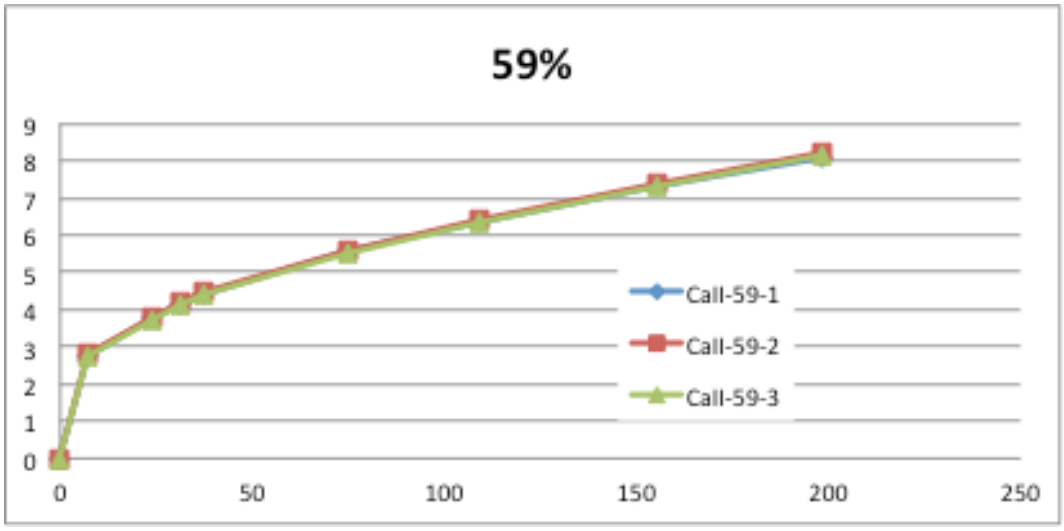

Fig. 22 Weight losses of the three cups with 59 % RH and discs CaII from mortar II.

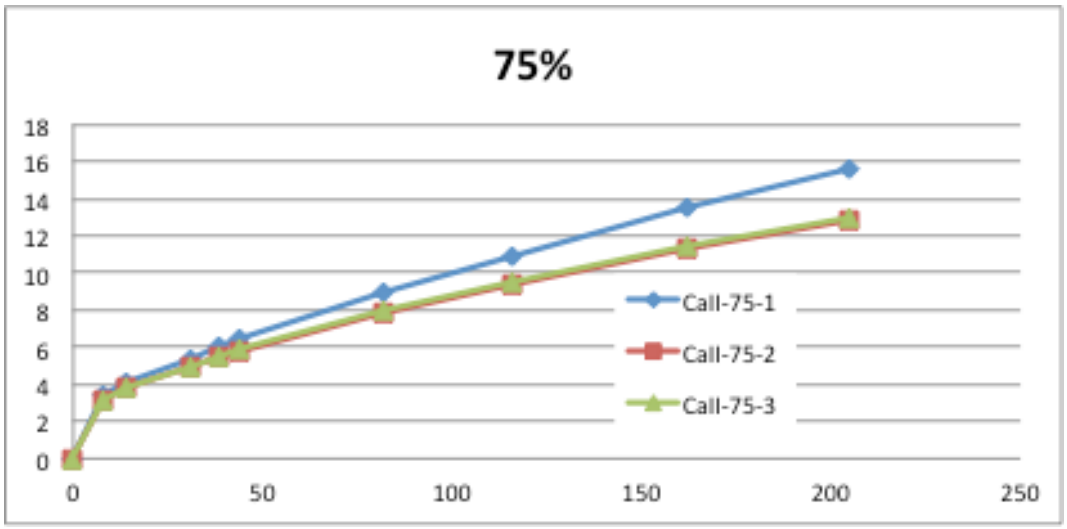

Fig. 23 Weight losses of the three cups with 75 % RH and discs CaII from mortar II.

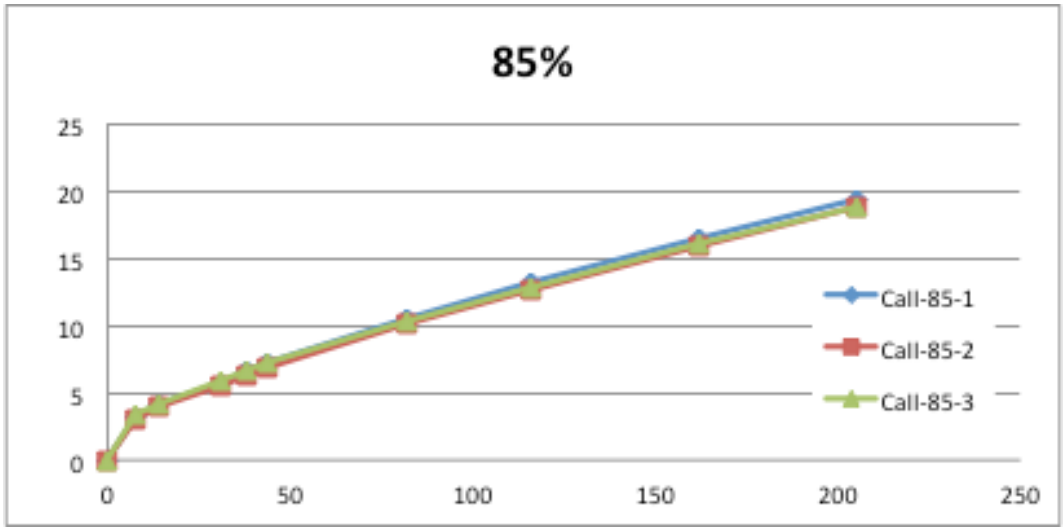

Fig. 24 Weight losses of the three cups with 85 % RH and discs CaII from mortar II.

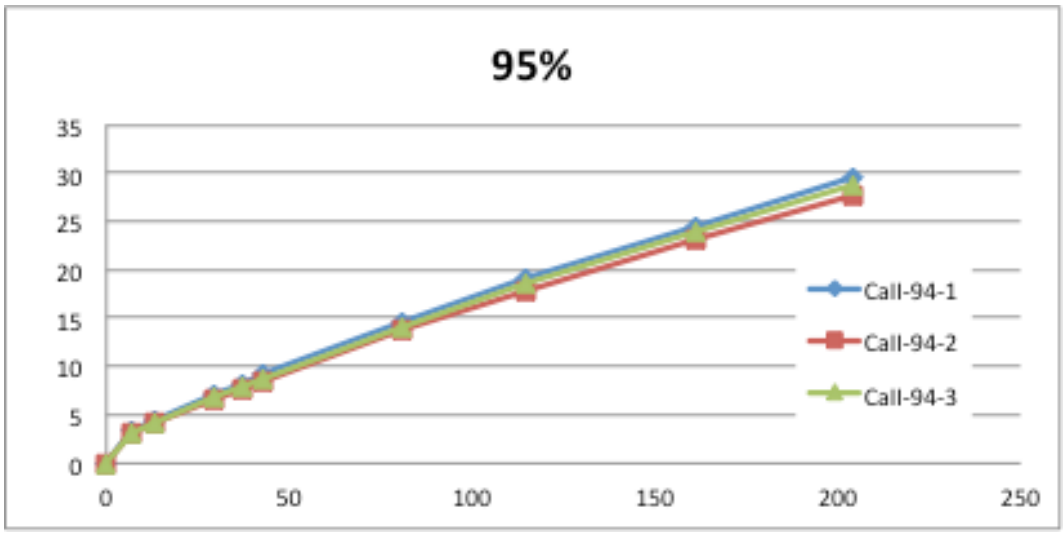

Fig. 25 Weight losses of the three cups with 95 % RH and discs CaII from mortar II.

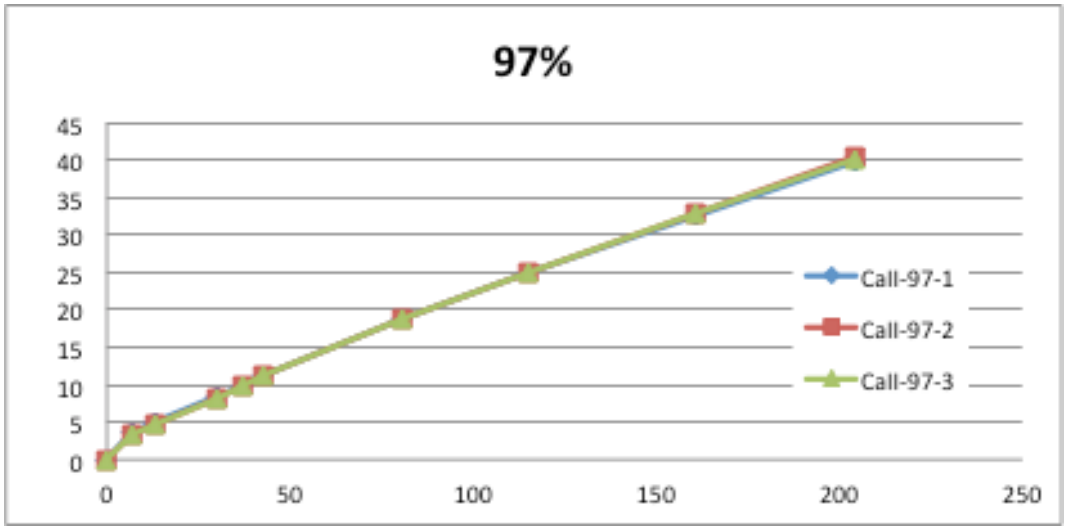

Fig. 26 Weight losses of the three cups with 97 % RH and discs CaII from mortar II.

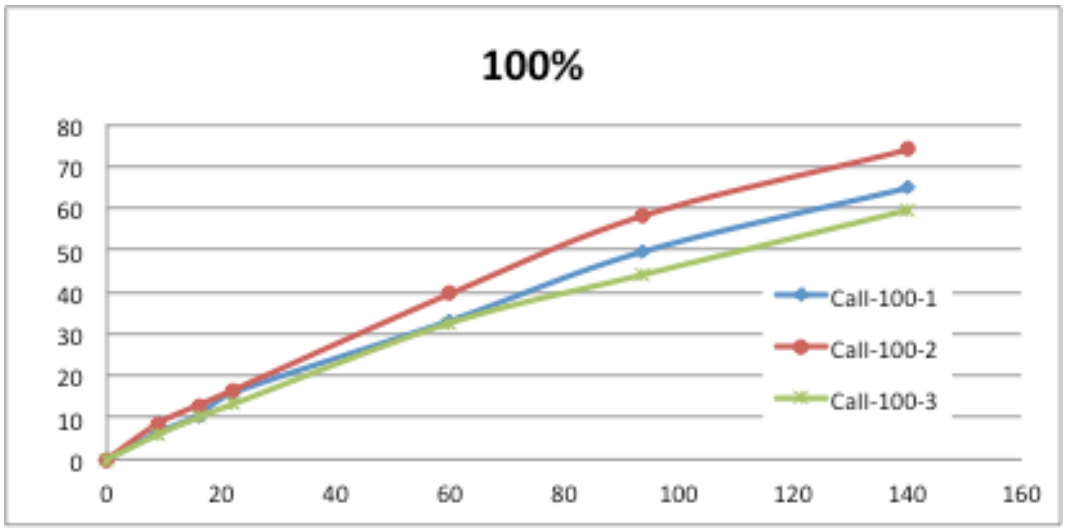

Fig. 27 Weight losses of the three "inverted cups" with 100 % RH and discs CaII from mortar II.

4.4 Evaluation of steady-state fluxes, average δ and PSI

The evaluation of the steady-state fluxes started by fitting straight lines to the last 100 days of average weight changes, cf. figure 28 and 29.

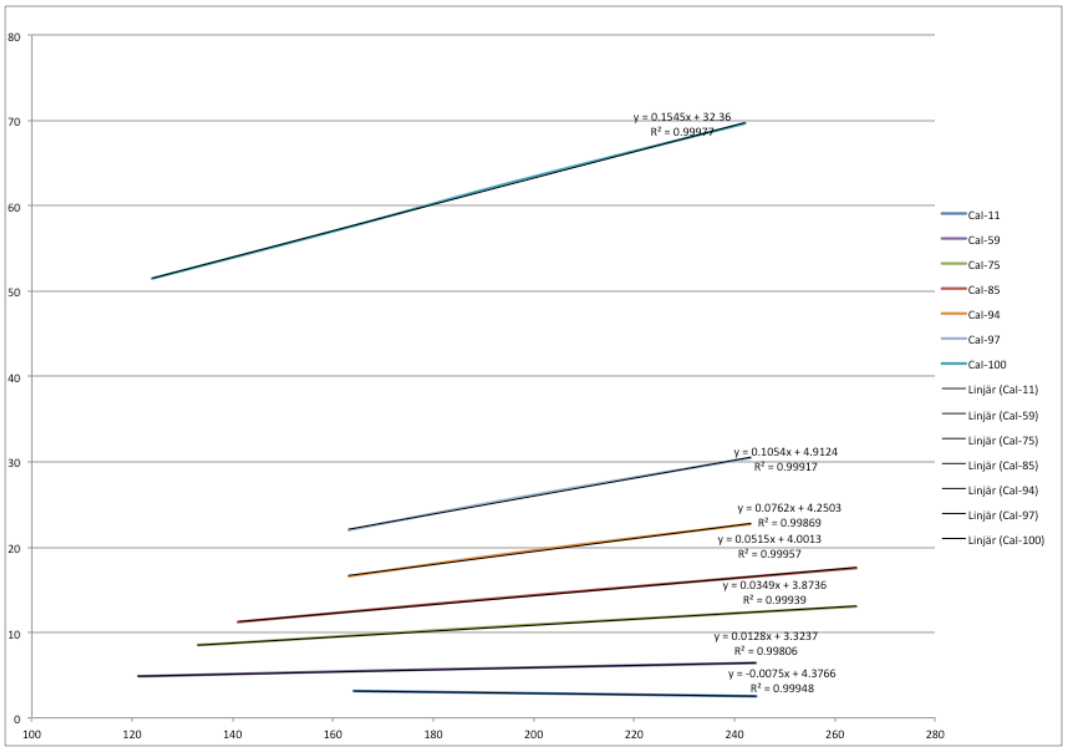

Fig. 28 Weight losses of the cups with mortar I during the steady-state period.

From the slope of these lines and the area of the discs the moisture flux J [kg/(m^{2}s)] is easily evaluated. The flux and the thickness of the air gap are then used to evaluate the RH Φ_2 at the inner surface of the discs with equation (13).

Finally, the average δ and the fundamental potential PSI are evaluated, in a series of RH intervals, using equations (12) and (8), respectively. The results are summarized in Table III.

PSI is shown in figure 30 and the average of δ in figure 31.

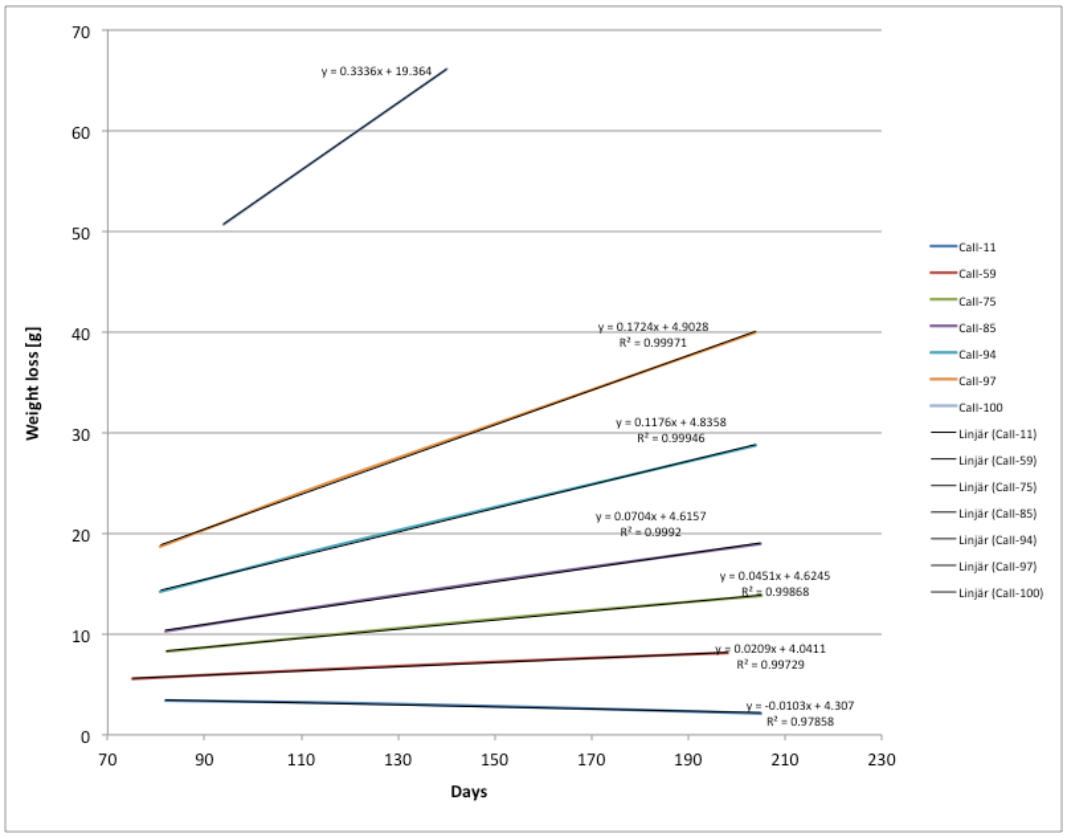

Fig. 29 Weight losses of the cups with mortar II during the steady-state period.

Table III. First step of the evaluation of the cup measurements

RH_{salt}	Flux		RH Φ_2		$\delta(33,\Phi_2)$		PSI(33,Φ_2)	
%	10^{-8} kg/m^{2}s		%		10^{-7} m^2/s		10^{-9} kg/ms	
mortar	I	II	I	II	I	II	I	II
11.0	-1.24	-1.71	11.09	11.12	0.49	0.68	-0.18	-0.26
33.0	0	0	33.00	33.00			0	0
59.0	2.11	3.46	58.85	58.76	0.71	1.16	0.32	0.52
75.0	5.78	7.47	74.60	74.48	1.20	1.56	0.87	1.12
85.0	8.53	11.7	84.41	84.19	1.44	1.97	1.28	1.75
94.7	12.6	19.5	93.83	93.35	1.80	2.80	1.89	2.92
97.0	17.4	28.5	95.79	95.02	2.41	3.99	2.62	4.28
100.0	25.6	55.2	100.0	100.0	3.31	7.15	3.84	8.28

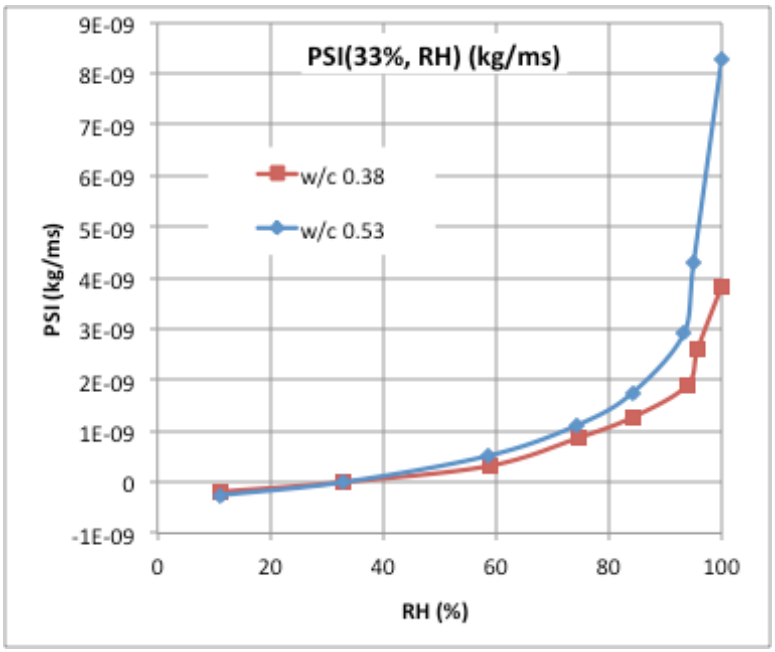

Fig. 30 The fundamental potential PSI as a function of the RH-interval with 33 % RH on one side and RH on the other side.

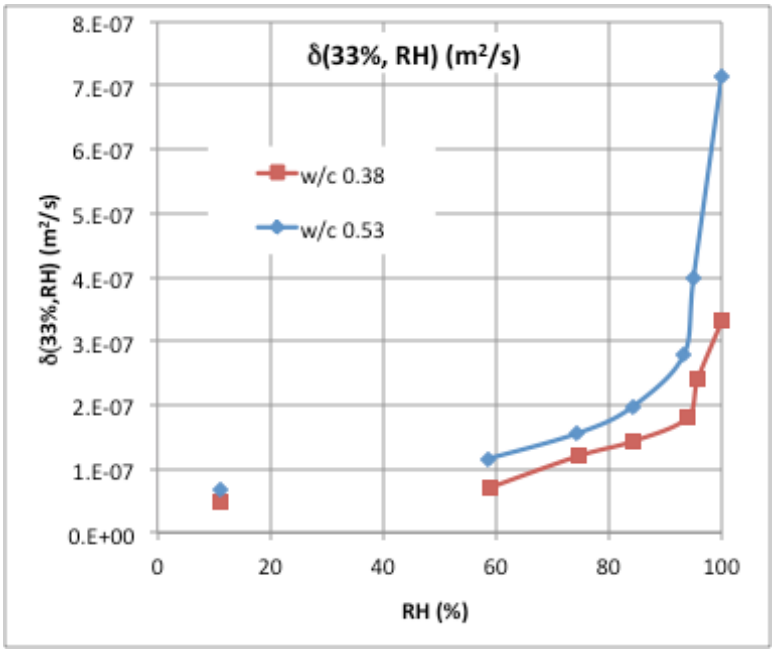

Fig. 31 The average moisture transport coefficient $\delta(33,\Phi_2)$ as a function of the RH-interval with 33 % RH on one side and RH=Φ_2 on the other side.

4.5 Evaluation of the moisture dependency of δ(RH)

The moisture transport coefficients $\delta(33, RH)$ in section 4.4 are the average values in large RH-intervals. These should be translated into moisture transport coefficients in much smaller RH-intervals or even as a function of RH in a point. The latter is done by simply derivate the curve showing the flux vs. RH, cf. Nilsson (1980). The uncertainty of such a derivation is, however, pretty large. Instead an evaluation can be done between the intervals used in the experiments.

Anderberg & Wadsö (2005) presented a method to evaluate the moisture transport coefficients in intervals between the ones where measurements were done, cf. figure 32.

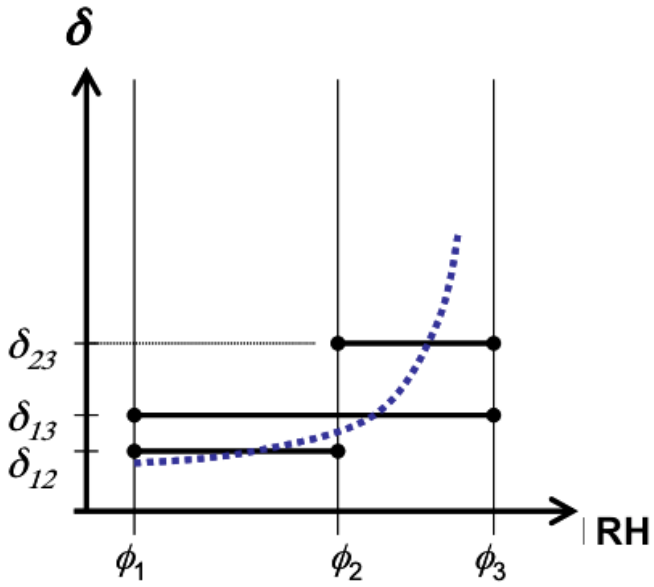

Fig. 32 The moisture transport coefficient δ(RH) (dashed curve) and the average $\delta_{ij}(RH_i, RH_j)$ in different intervals

Translated into the symbols used here, their equation for the moisture transport coefficient $\delta_{23}(\phi_2, \phi_3)$ in an RH-interval (ϕ_2, ϕ_3) becomes

$$\bar{\delta}_{23} = \frac{\bar{\delta}_{13}\left(\phi_3 - \phi_1\right) - \bar{\delta}_{12}\left(\phi_2 - \phi_1\right)}{\phi_3 - \phi_2} \tag{17}$$

By using this equation, the average $\delta_{ij}(RH_i, RH_j)$ in the large intervals with 33 % RH as one interval border can be recalculated into average δ in much smaller intervals. The results of these calculations are shown in Table IV and in figure 33.

Table IV. The average $\delta_{ij}(\Phi_1, \Phi_2)$ in small RH intervals

RH Φ_1 (%)		RH Φ_2 (%)		$\delta(\Phi_1,\Phi_2)$ (10^{-7} m^2/s)	
I	II	I	II	I	II
11.09	11.12	33.00	33.00	0.49	0.68
33.00	33.00	58.85	58.76	0.71	1.16
58.85	58.76	74.60	74.48	2.01	2.21
74.60	74.48	84.41	84.19	1.81	2.64
84.41	84.19	93.83	93.35	2.17	3.65
93.83	93.35	95.79	95.02	4.99	9.02
95.79	95.02	100.0	100.0	4.00	9.57

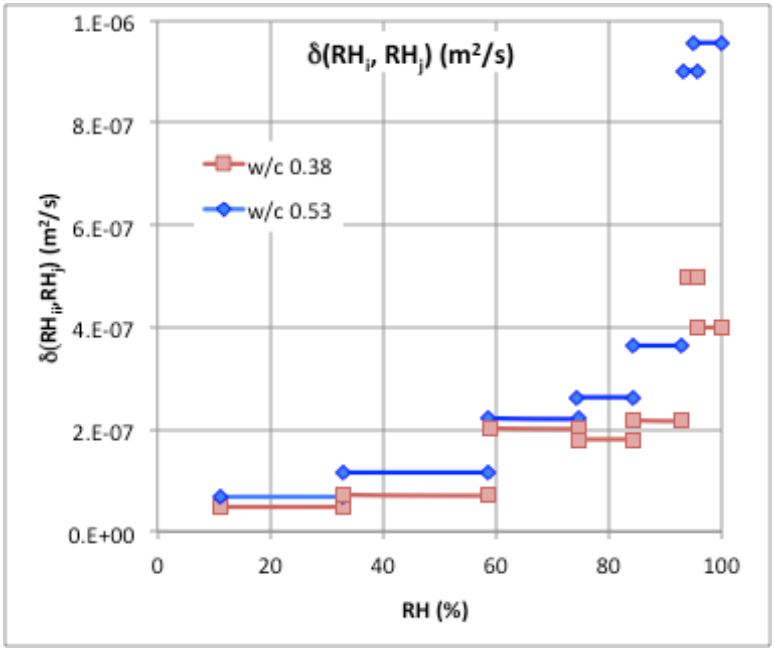

Fig. 33 The average moisture transport coefficient $\delta_{ij}(RH_i, RH_j)$ in small RH intervals for the two mortars.

A comparison between figure 30 and figure 33 shows the advantage with the fundamental potential PSI. PSI is the direct flux measurements and the uncertainties in the flux measurements are directly shown in the results. The uncertainties of the moisture transport coefficients δ in small intervals are also affected by the uncertainties in the evaluation of the borders of the RH intervals. In a small RH interval these uncertainties will have a larger effect on

the evaluated δ. This is clearly shown in figure 33, where δ is almost the same in three neighbouring RH-intervals for the mortar with w/C=0.38 and the δ is larger at a lower RH than closer to 100 % RH, but in a very small RH interval.

4.6 Conclusions on cup methods

The cup methods are easy to use, are reliable and are fairly rapid. They need a stable, surrounding, CO_2-free climate, however, which can be difficult to maintain during longer periods of time.

Evaluating the fundamental potential PSI is very simple and eliminates the derivation that adds to the uncertainty of the moisture transport coefficient δ.

5 Steady-state moisture profile method

5.1 Experimental set-up

The specimens shown to the right in figure 12 were used for a steady-state moisture profile experiment. "Rolls" of five 15 mm thick discs with a diameter of 50 mm and edge sealed were used. A thin cloth of cotton was placed between the discs to ensure a good "moisture contact" between the discs. The circumference of these "rolls" was also sealed with a rubber-bitumen-aluminium tape to ensure 1D moisture transport during drying and steady-state moisture flow.

A glass cup with water was attached on top of each roll and the rolls were placed in a climate box with 33 % RH, originally. The rolls were wet cured before the experiment started. One roll was used for each mortar.

5.2 Flux measurements

The weight changes of the rolls were followed for almost two years. One of the rolls obviously had a leakage that was not observed until the end of the experiment. The results for the other roll, with discs from mortar II, are shown in figure 34.

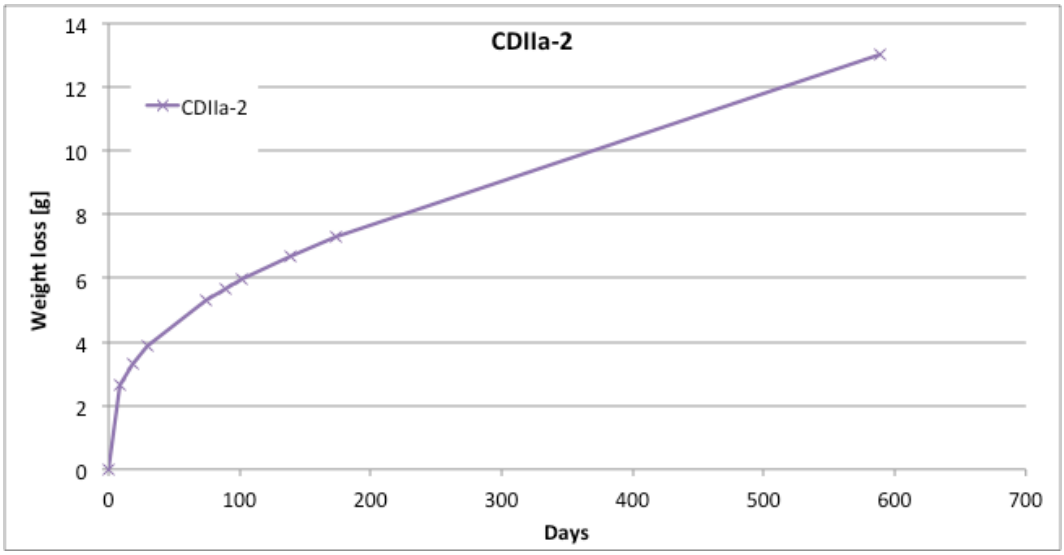

Fig. 34 Weight changes of the roll of five discs from mortar II due to drying and, eventually, steady-state flux

From the final weight changes, the steady-state flux was evaluated. Since the RH in the climate box gradually changed during the two years, an RH of 50 %

is used for the evaluation of the average moisture transport coefficient and the fundamental potential. The results are shown in Table V.

Table V. Evaluation of average values from the steady-state moisture profile method, mortar II (w/c=0.53)

Flux J	$\delta_{av}(53, 100)$	PSI, $\Psi(53, 100)$
kg/m^{2}s	10^{-7}m^2/s	10^{-9}kg/ms
$8.06 \cdot 10^{-8}$	7.4	6.0
(From cup methods) (33, 100)	(9.6)	(8.3)

A comparison is made in table V with the results from the cup method, cf. table III. The comparison, however, is in slightly different RH intervals; (33-100) with the cup methods and (53, 100) here. Obviously, the comparison shows similar results.

5.3 Moisture profile measurements

After completion of the experiments, the steady-state moisture profile was to be determined. Attempts were made to do this in three different ways:

1. Moisture content of each disc,
2. RH at the two surfaces of each disc
3. RH of the cloth between two discs.

5.3.1 Moisture content profiles

After RH had been measured at the surfaces of the discs, see below, the moisture ratios of the discs were determined, from the weights before and after drying at +105°C. From the moisture contents and the original densities of each disc the moisture contents were calculated. The results are given in table VI and figure 35.

Table VI. The moisture ratios and moisture contents of the discs; mortar II.

Disc	Height (mm) from bottom (dry) surface	Moisture ratio u (% by weight)	Moisture content (kg/m^3)
20-2	7.5	4.1	86.8
20-4	22.5	5.4	114.0
20-6	37.5	5.8	121.6
20-7	52.5	3.7	78.5
20-8	67.5	5.1	107.5

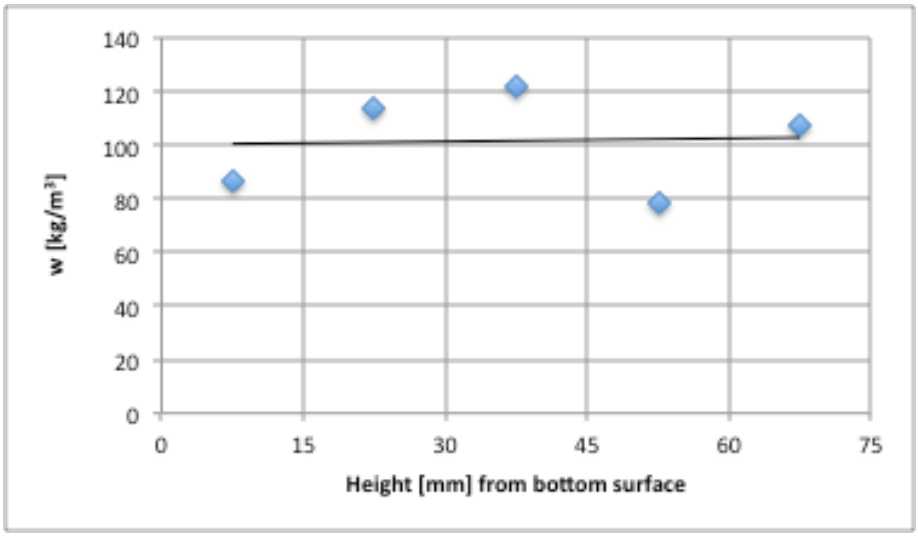

Fig. 35 Steady-state moisture content distribution after 589 days

Obviously, the moisture content measurements give too large scatter, even when measured on mortars.

5.3.2 RH-profiles

RH was measured in two ways, with carefully calibrated Vaisala RH-probes. To be able to measure RH at the surfaces of the discs a number of glass cups were manufactured with the same diameter as the discs. A small tube was attached into the glass cups from the side. The tubes had a diameter that fitted the Vaisala RH-probes. With these tubes RH could be measured at a surface of a disc by putting a glass cup at the surface and seal the edges. Then an RH-probe was inserted and the RH was read the day after.

The cloths between the discs had of course adjusted its moisture content to be in equilibrium with the disc surfaces. Even though the weight of a piece of cloth is small, there is a possibility to measure RH of the cloth by putting it into a glass test tube and insert an RH-probe.

In this way RH could be measured at a certain depth, between two discs, in three ways: on the cloth, on the "drier" surface and on the "wetter" of the two surfaces. The results are shown in table VII and in figure 36.

From the data in table VII and figure 36 it is obvious that the measurements on the cloths had to large systematic errors. The RH is some 3-4 % RH too low.

The RH:s measured at the surface of the discs have also systematic errors. In each disc there is a moisture profile and a steady-state flux of moisture. When sealing a surface for a day or two for the RH-measurement, the flux to/from a surface will be zero immediately. This will change the moisture profile in the disc in such a way that an "upstream" surface will dry and a "downstream" surface will get a rise in RH during the measurement. From the results it

seems as if the measurements on the "dry" surfaces have larger systematic errors.

Table VII. RH measured between the five discs, mortar II.

Disc	Depth (mm)	Wetter surface	Drier surface	Cloths
	0		52.7	
20-2				
	15	73.6	72.6	69.5
20-4				
	30	83.6/84.9	81.0	77.5
20-6				
	45	91.8	79.9	85.1
20-7				
	60	97.8	87.9	94.3
20-8				
	75	100		

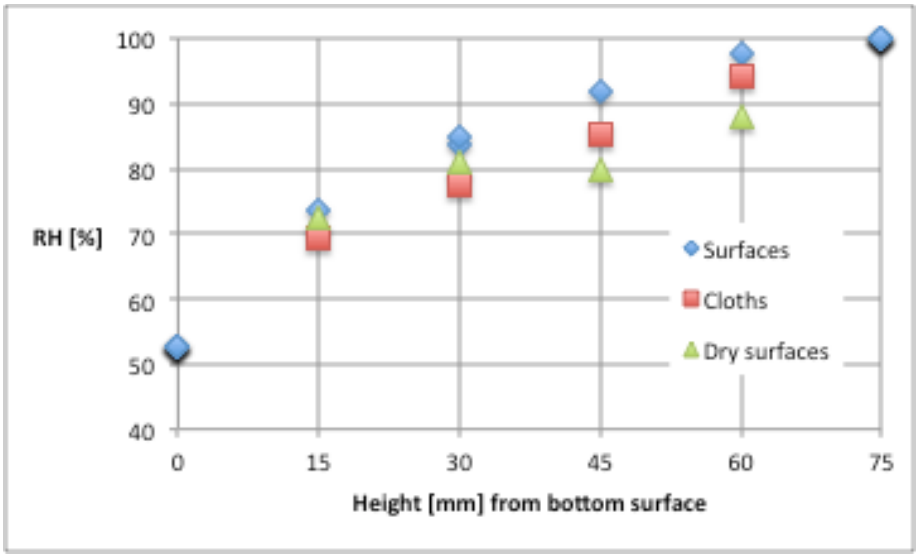

Fig. 36 Measured steady-state RH between the five discs

The RH:s measured at the "wetter" surfaces at the discs are displayed in figure 37 and a trend-line is fitted to the points.

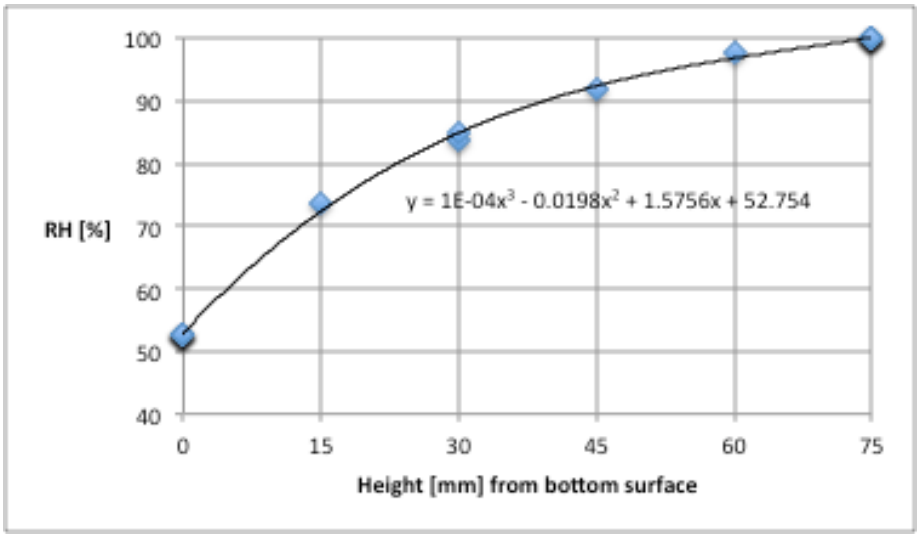

Fig. 37 The steady-state RH-profile through the five discs after 589 days

From the trendline the moisture transport properties are evaluated. The curve is derivated at some points. From the slope and the flux in these points, the moisture transport coefficient δ is calculated by equation (7). The fundamental potential PSI is calculated in each point from the flux and the thickness up to that point, with equation (8).

The results are given in table VIII and shown in figure 38 and 39.

Table VIII. Evaluation of the steady-state RH-profile, mortar II.

x (mm)	dRH/dx [%/mm]	RH (%)	δ(RF) m^2/s	PSI
0	1.576	52.8	$2.96 \cdot 10^{-7}$	0
8	1.277	64.1	$3.65 \cdot 10^{-7}$	$6.45 \cdot 10^{-10}$
15	1.046	72.3	$4.45 \cdot 10^{-7}$	$1.21 \cdot 10^{-9}$
22	0.844	78.9	$5.52 \cdot 10^{-7}$	$1.77 \cdot 10^{-9}$
30	0.647	84.8	$7.21 \cdot 10^{-7}$	$2.42 \cdot 10^{-9}$
45	0.377	92.3	$1.24 \cdot 10^{-6}$	$3.63 \cdot 10^{-9}$
60	0.236	96.7	$1.97 \cdot 10^{-6}$	$4.84 \cdot 10^{-9}$
65	0.218	97.9	$2.13 \cdot 10^{-6}$	$5.24 \cdot 10^{-9}$

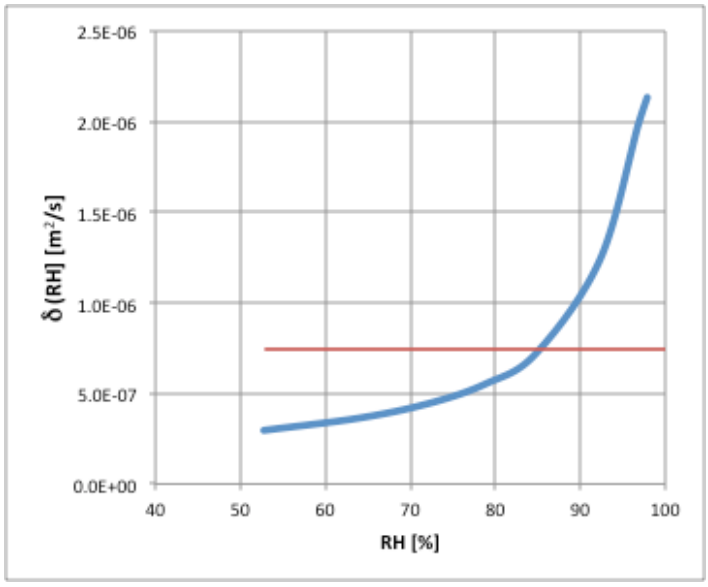

Fig. 38 The moisture transport coefficient δ(RH) as evaluated from the steady-state flux and RH-profiles. The horizontal line is the average δ(53,100) in the whole RH-interval

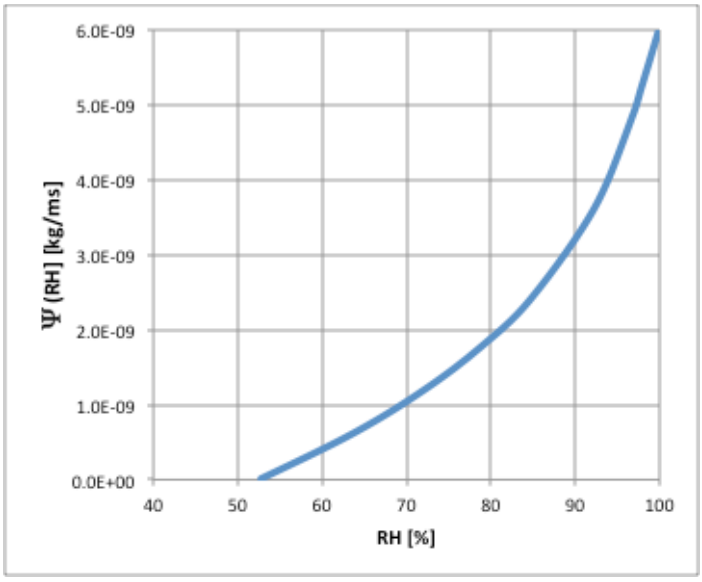

Fig. 39 The fundamental potential PSI, Ψ(53, RH), as evaluated from the steady-state flux and RH-profiles

A comparison is made in figure 40 and 41 between the moisture transport coefficients determined by the cup method and by the steady-state profile method. There is a significant difference between the moisture transport coefficients δ(RH) from the two methods. The results from the cup method are very sensitive to the RH-intervals on the two sides of a disc. The results from the steady-state moisture profile method are very sensitive to how the

slope of the RH-profile is evaluated. The average coefficients in a large interval are very close, cf. table V, bearing in mind that the interval is somewhat larger for the cup method.

The comparison of the fundamental potentials from the two methods looks much better.

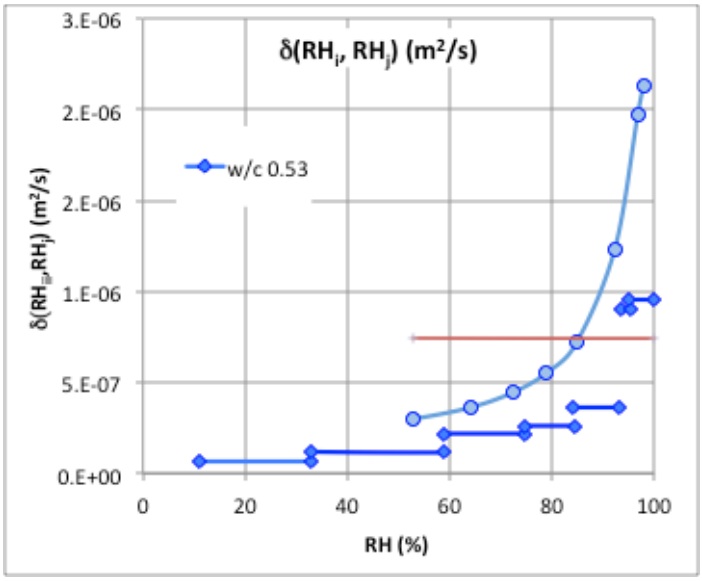

Fig. 40 A comparison between the moisture transport coefficients δ(RH) from the cup method (horizontal lines) and the steady-state moisture profile method (curve).

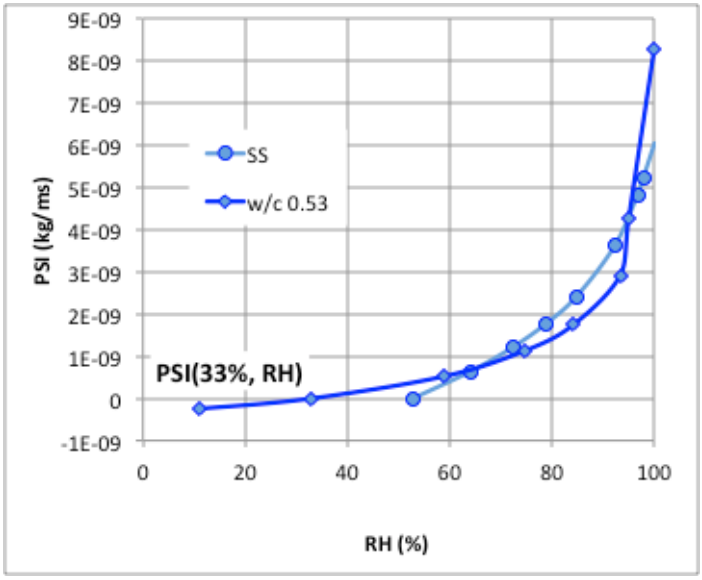

Fig. 41 A comparison between the fundamental potentials Ψ(RH) from the cup method (diamonds) and the steady-state moisture profile method (circles).

6 Non steady-state moisture profile method

6.1 Experimental set-up

The specimens shown to the left in figure 12 were used for a non-steady-state moisture profile experiment. "Rolls" of five 15 mm thick discs with a diameter of 50 mm and edge sealed were used. A thin cloth of cotton was placed between the discs to ensure a good "moisture contact" between the discs. The circumference of these "rolls" was also sealed with a rubber-bitumen-aluminium tape to ensure 1D moisture transport during drying.

The rolls were placed in a climate box with +20°C 33 % RH, originally. The rolls were wet cured before the experiment started. One roll was used for each mortar.

6.2 Weight measurements

The weight changes of the rolls were followed for almost two years. The results for the two rolls, with discs from mortars I and II, are shown in figure 42.

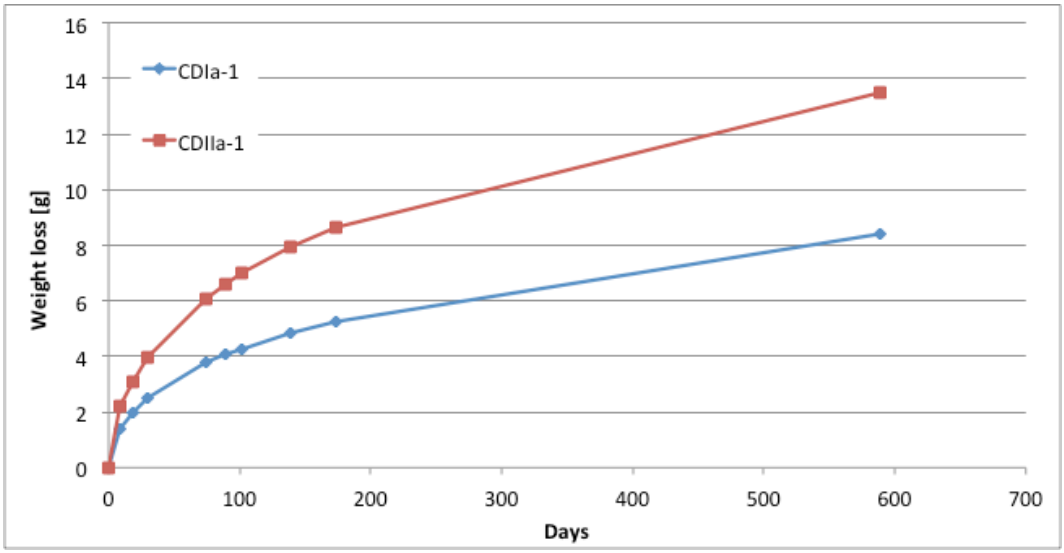

Fig. 42 Weight changes of the two rolls of five discs due to drying

Since the RH in the climate box gradually changed during the two years, an RH of 50 % was used as the surrounding climate. The final weight loss was far from equilibrium with the surrounding climate. This is a decisive parameter in the evaluation of non-steady-state experiments. The desorption isotherms for

the mortars, see figure 43, were used to calculate the expected, final weight loss.

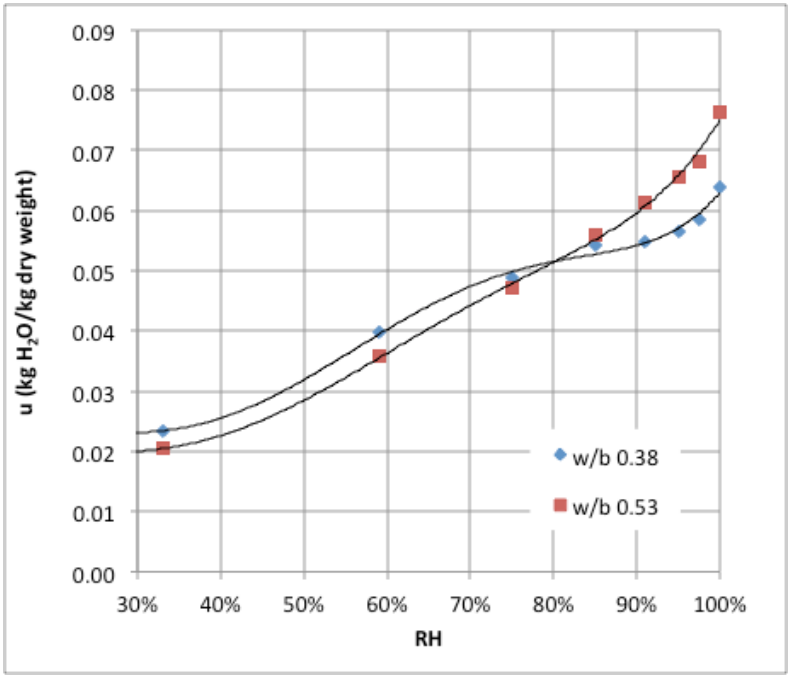

Fig. 43 Desorption isotherms for the two mortars. Data from Olsson et al (2012)

6.3 Moisture profile measurements

After completion of the experiments, the moisture profile was to be determined. Attempts were made to do this in three different ways:

1. Moisture content of each disc,
2. RH at the two surfaces of each disc
3. RH of the cloth between two discs.

6.3.1 Moisture content profiles

The moisture content of each disc was calculated from the moisture ratio and the original density as explained in section 5.3.1. The results are shown in figure 44.

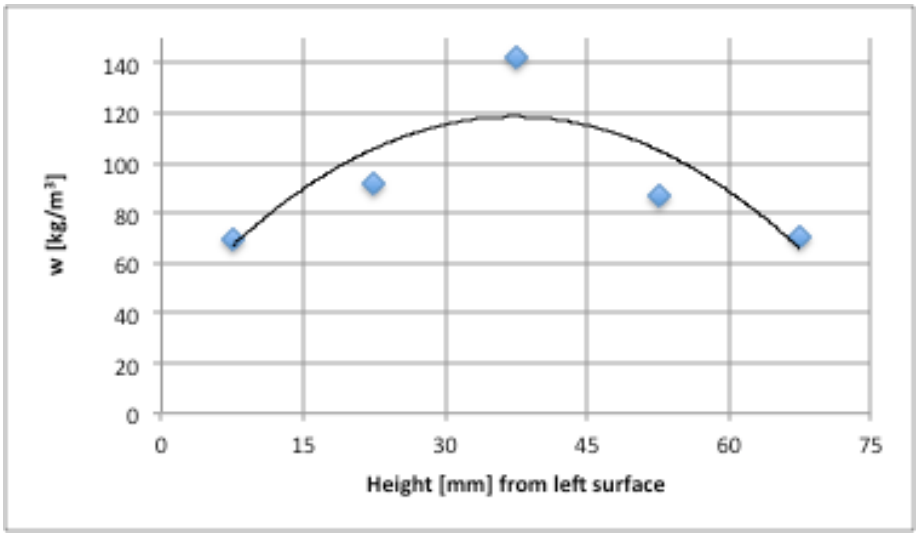

Fig. 44 Moisture content distribution after 589 days

Obviously, the moisture content measurements give too large scatter, even when measured on mortars, in the same way as in section 5.3.1.

6.3.2 RH-profiles

RH between the discs was measured in the same way as in section 5.3.2. The results are shown in table IX, in figure 45 and figure 46.

Table IX. RH measured between the five discs of the two mortar rolls.

Disc		Depth (mm)	Wetter surface		Drier surface		Cloths	
I	II		I	II	I	II	I	II
		0			55.2	52.3		
17-1	10-1							
		15	61.2	57.9	58.5	-	60.7	57.5
17-2	10-2							
		30	65.6	61.0	63.0	59.0	62.6	67.4
17-5	10-6							
		45	63.9	59.6	60.7	-	60.9	72.1
17-6								
		60	60.7	-	59.1	-	59.3	-
17-8								
		75			51.5	-		

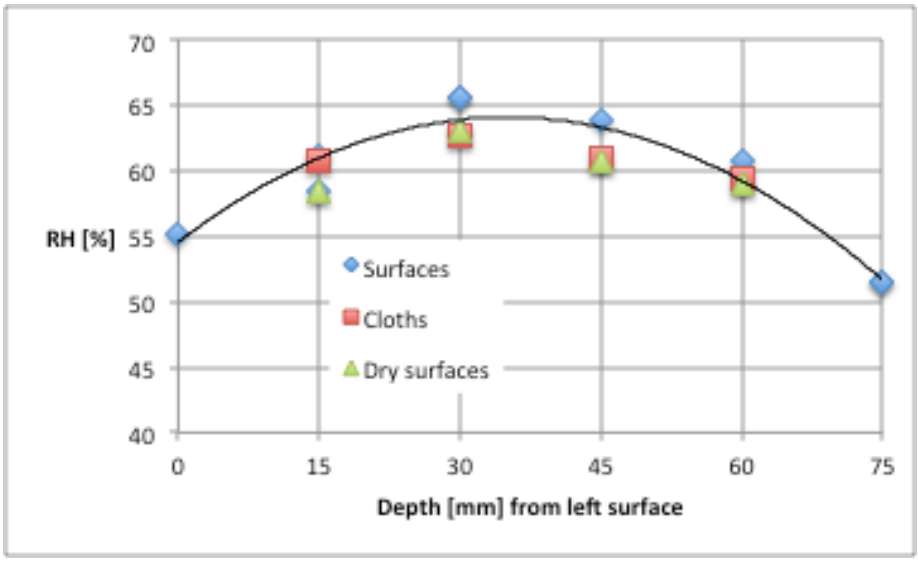

Figure 45 Measured RH between the five discs, mortar I

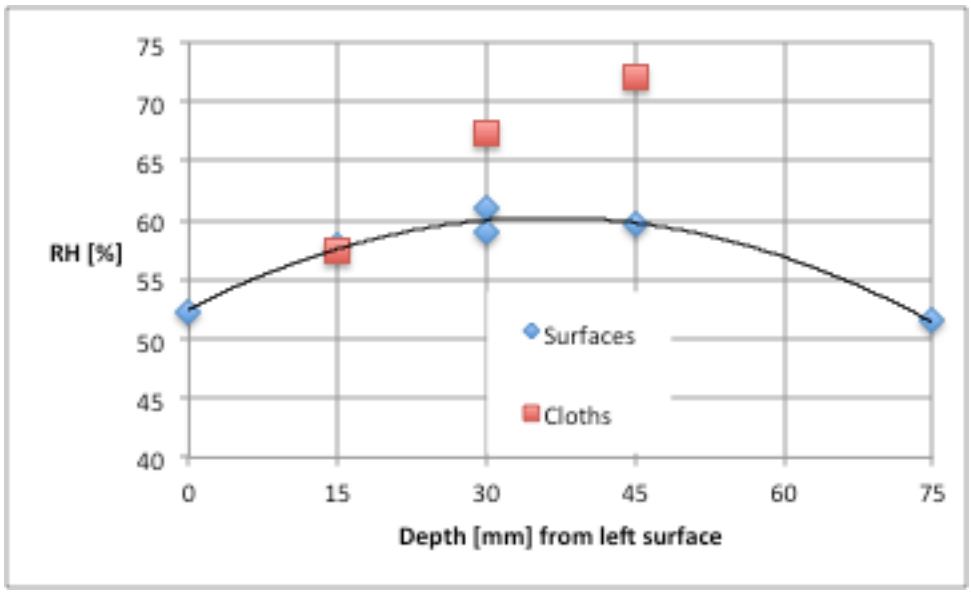

Figure 46 Measured RH between the five discs, mortar II

6.4 Evaluation

After completion of the experiments, the moisture profile was to be compared to predicted profiles like the ones in figure 47. From that comparison, the diffusivity might be evaluated.

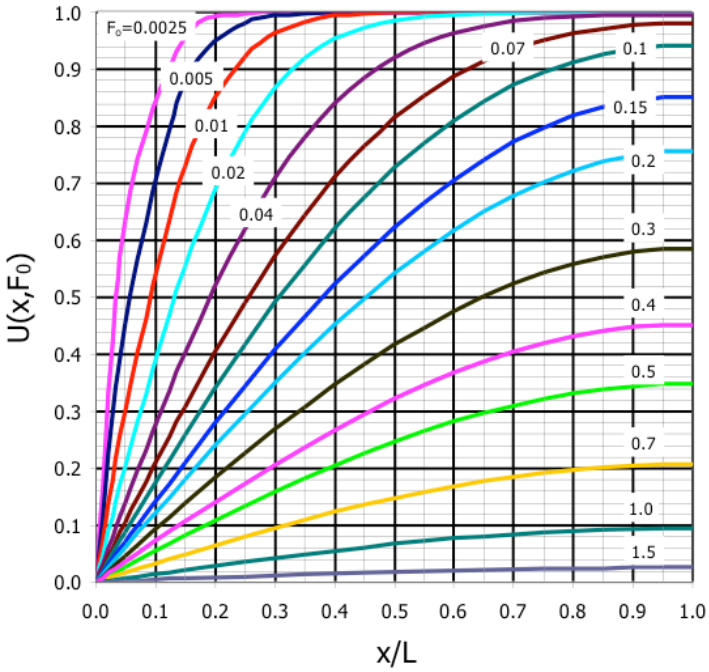

Fig. 47 The solution of the mass balance equation (14) for one-sided drying with a constant moisture diffusivity D_w

In figure 47, the Fourier Number F_0 is the same as in equation (16). The "drying potential" U is different from the one (U_m) in equation (15), that was based on the average moisture content. Here U is based on the moisture content at different depths, i.e. the moisture profile. The definition is

$$U(x,F_0) = \frac{w(x) - w_\infty}{w_0 - w_\infty} \tag{18}$$

To be able to use figure 47, the RH-profiles must be translated into moisture content profiles. This is done by using the sorption isotherm. Only the top values in the profiles are used. The sorption isotherm in figure 43 is used, with the moisture content u as moisture ratio in % by dry weight.

The time t is 589 days and L is half the thickness of the rolls.

Table X. Evaluation of RH-profiles in figures 45 & 46

Mortar	RH_{top}	u(x=L)	u_∞	u_0	$U(x,F_0)$	F_0 *(Fig. 47)*	L *(m)*	D_w (m^2/s)
I	64 %	4.4	3.2	6.4	0.38	0.47	0.0375	$1.1 \cdot 10^{-11}$
II	60 %	6.3	2.8	7.6	0.10	1.0	0.0375	$2.4 \cdot 10^{-11}$

Note that the assumption here is that D_w is a constant.

7 Non steady-state sorption method

7.1 Experiments

The non-steady state sorption method was applied to mortar specimens with thicknesses of 75, 45 and 15 mm that were dried in climate boxes. The specimens and experimental results are first shown. The individual experimental series are then evaluated and compared.

7.2 2L=75 mm

The rolls with five 15 mm mortar discs that dried two ways, cf. section 6.1, have a characteristic thickness L of 75/2=37.5 mm. The drying curves for the two rolls were shown in figure 42. The curves were evaluated with the desorption isotherms in section 6.2 to get the final weight loss. From that the drying potential U_m could be derived. The data is shown in table XI.

Table XI. Data from drying of rolls with thicknesses 2L=75 mm

Time	Weight loss (g)		t/L^2	*1-*U_m		U_m	
(days)	CDIa-1	CDIIa-1	(10^9 s/m^2)	CDIa-1	CDIIa-1	CDIa-1	CDIIa-1
0	0	0	0	0	0	0	0
9	1.39	2.20	0.553	0.104	0.129	0.896	0.871
18	1.98	3.10	1.11	0.148	0.181	0.851	0.819
30	2.52	3.99	1.84	0.189	0.233	0.811	0.767
74	3.76	6.07	4.55	0.282	0.355	0.718	0.645
89	4.06	6.61	5.47	0.305	0.387	0.695	0.613
102	4.28	7.00	6.27	0.321	0.410	0.679	0.590
139	4.83	7.94	8.54	0.363	0.465	0.637	0.535
173	5.23	8.63	10.62	0.393	0.505	0.607	0.495
589	8.42	13.50	36.18	0.632	0.790	0.368	0.210
∞	13.32	17.09	∞	1	1	1	1

The U_m-values and t/L^2-values in table XI have been fitted to the analytical solution in figure 8. This was done by fitting the data with the curve at U_m=0.5 by changing the diffusivity D_w to get a suitable Fourier number F_0. The results are shown in figure 48.

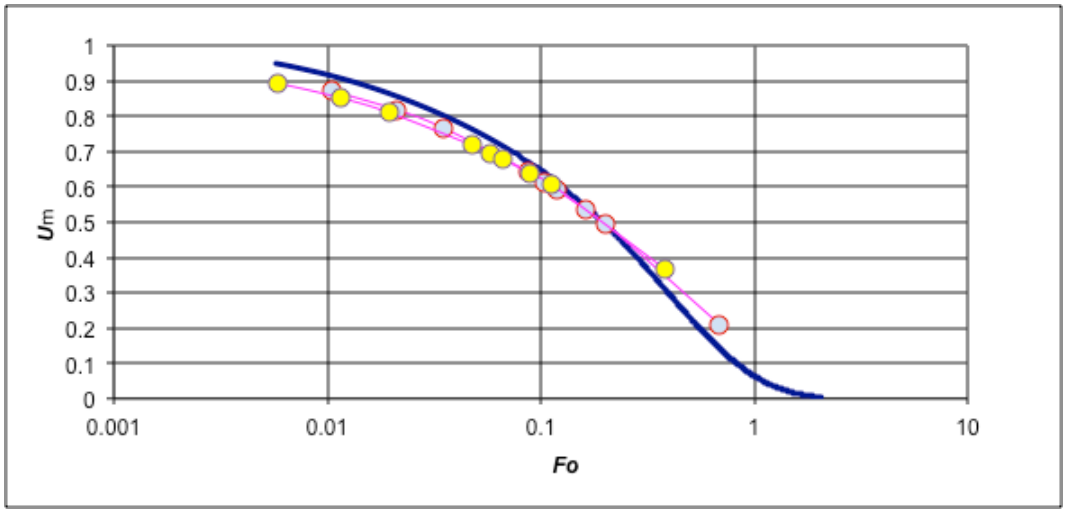

Fig. 48 The weight loss curves for the two specimens of five 15 mm mortar rolls drying two ways, cf. table XI, fitted to the analytical solution with a constant diffusivities D_w at U_m=0.5

Table XII. Evaluation of sorption curves in figure 48

Mortar	$U_m(F_0)$	D_w (m^2/s)
I	0.50	$1.05 \cdot 10^{-11}$
II	0.50	$1.90 \cdot 10^{-11}$

Note that the assumption here is that D_w is a constant in the whole RH interval.

From figure 48 it is obvious that the data do not fit the analytical solution with a constant diffusivity D_w. An attempt was made to compare with a numerical solution with a non-constant D_w. A desorption isotherm and a transport coefficient as in figure 49 were used as a first assumption.

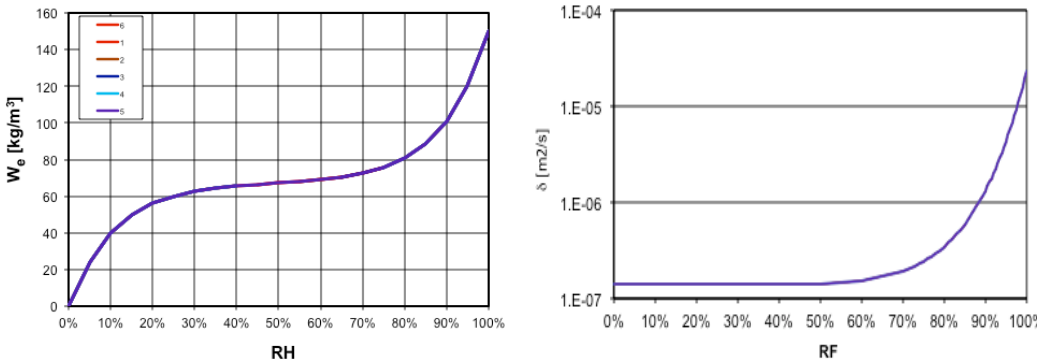

Fig. 49 The desorption isotherm and the transport coefficient δ(RH) used in a first attempt to compare data with a solution with a non-constant Dw

The diffusivity D_w can be calculated from the slope of the desorption isotherm dw/dφ and the transport coefficient by comparing equations (5) and (9)

$$J = -\delta(\varphi)\frac{\partial v}{\partial x} = -D_w(\varphi)\frac{\partial w}{\partial x}$$

$$D_w(\varphi) = \delta(\varphi)\cdot\frac{v_s}{\frac{dw}{d\varphi}(\varphi)} \qquad (19)$$

From the data in figure 49 the calculated diffusivity D_w will be according to figure 50.

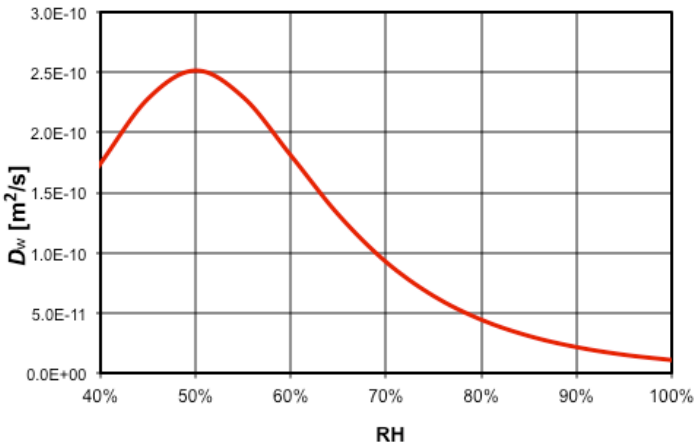

Fig. 50 The diffusivity calculated from equation (19) and the desorption isotherm and the transport coefficient δ(RH) in figure 49.

With the input data in figure 49 a numerical solution was calculated by a finite difference method with constant surrounding climatic conditions. The result of this calculation was then "translated" into Fourier numbers F_0 and drying potentials U_m. The solution was then fitted to the experimental data by adjusting the absolute levels of the transport coefficient to make the data fit the solution at U_m=0.5.

The results of this fitting procedure are shown in figure 51. The evaluation of the diffusivities are given in table XIII.

Table XIII. Evaluation of sorption curves in figure 51

Mortar	$U_m(F_0)$	*"Average"* D_w (m^2/s)
I	0.50	$1.3\cdot10^{-11}$
II	0.50	$2.4\cdot10^{-11}$

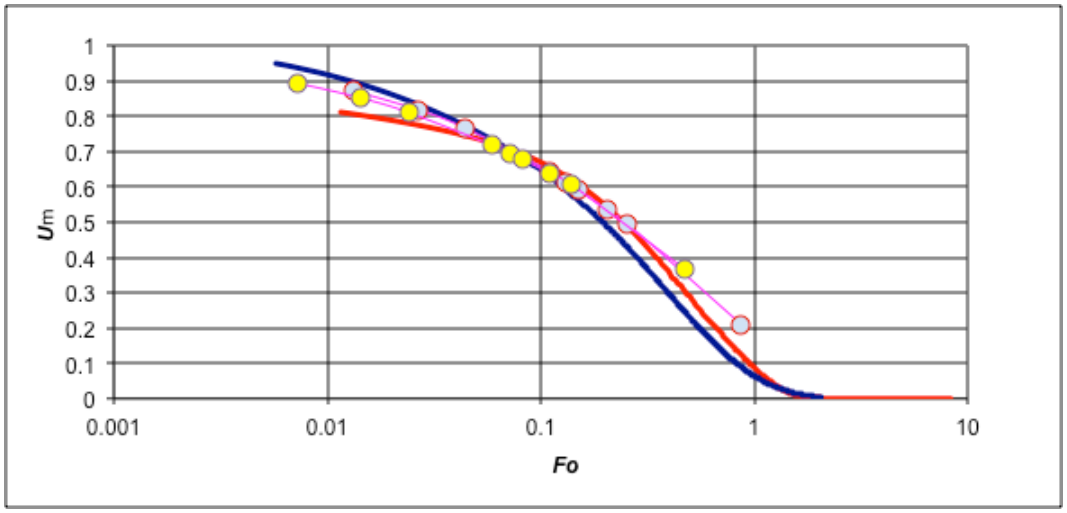

Fig. 51 The weight loss curves for the two specimens of five 15 mm mortar rolls drying two ways, cf. table XI, fitted to a numerical solution (red curve) with non-constant diffusivities D_w at U_m=0.5.

The "average" diffusivity derived in this way is of course a strange average since it is a diffusivity number that makes the drying process fit the numerical solution at U_m=0.5.

From figure 51 it is seen that the fit is far from perfect. In the beginning of the drying process the numerical solution with a non-constant D_w gives a too fast drying while at the end of the drying process the drying rate is over-estimated. Further attempts should be done with new assumptions of the shape of the desorption isotherm.

7.3 2L=15 and 45 mm

The discs with 15 and 45 mm mortar discs that dried two ways, cf. section 6.1, have a characteristic thickness L of 7.5 and 22.5 mm, respectively. The drying curves for the discs are shown in figure 52 and 53. The curves were evaluated with the desorption isotherms in section 6.1. The evaluated diffusivities are shown in table XIV.

Table XIV. Evaluation of sorption curves in figure 52 and 53

Mortar	$U_m(F_0)$	*"Average"* D_w (m^2/s)
I	0.50	$1.4 \cdot 10^{-11}$
II	0.50	$2.5 \cdot 10^{-11}$

From figures 52 and 53 it is obvious that the drying curves for the mortar discs with different thicknesses do not coincide perfectly, as they should, at least not for the mortar II, with a w/c of 0.53.

Table XV. Diffusivities from different methods

Method	*Section*	*"Average" D_w* (m^2/s)	
		Mortar I	Mortar II
Moisture content profiles	6.3.1	(scatter too large)	
RH-profiles	6.3.2 & 6.4	$1.1 \cdot 10^{-11}$	$2.4 \cdot 10^{-11}$
Sorption method, 2L=75 mm; D_w constant	7.2	$1.05 \cdot 10^{-11}$	$1.90 \cdot 10^{-11}$
Ditto, RH-dependent D_w	7.2	$1.3 \cdot 10^{-11}$	$2.4 \cdot 10^{-11}$
Sorption method, 2L=15 & 45 mm; D_w constant and RH-dependent	7.3	$1.4 \cdot 10^{-11}$	$2.5 \cdot 10^{-11}$

The different methods gave roughly the same diffusivity for the two mortars and the methods clearly separated the moisture transport properties of the two mortars. Consequently, it seems as if "any method" to determine a diffusivity is fairly robust.

The uncertainties, however, are large and the fit between theory and experiments is not good enough. A crude conclusion would be that the sorption method might give somewhat different results with different thicknesses of the specimens. The experiments done used a too large RH interval to be able to evaluate the actual moisture dependency of the diffusivity. Several, narrower, intervals should have been used instead.

8 Conclusions

The following conclusions have been drawn from the experimental study.

a. The cup methods are easy to use, reliable and fairly rapid; need a stable, surrounding, CO_2-free climate, however. Evaluating the fundamental potential PSI is simple and eliminates the derivation that adds to the uncertainty
b. Steady-state moisture distribution measurements are very time-consuming and the RH-profiling is a delicate matter. Moisture contents are scattering.
c. Sorption experiments are very easy to perform but difficult to evaluate, because of the peculiar moisture-dependency of D_w and the difficulties in achieving equilibrium conditions. Initial uniform conditions are difficult to obtain for low w/c-materials, except to initial self-desiccation. Carbonation is difficult to avoid during long-term tests.
d. Sorption experiments in small steps are uncertain; the initial and final conditions are difficult to define properly.

No method[1] is quick enough for evaluating the age-dependency of moisture transport properties!

[1] except the pressure difference method applicable at t < 6 hours, cf. Radocea (1992)!

References

Anderberg, A. & Wadsö, L. (2005) *Moisture in Self-levelling Flooring Compounds. Part I. Diffusion Coefficients*. Nordic Concrete Research 32, pp. 3–15.

Baroghel-Bouny, V. (2007) Water vapour sorption experiments on hardened cementitious materials. Part II: Essential tool for assessment of transport properties and for durability prediction. Cement & Concrete Research 37 (2007) 438–454.

Hedenblad, G. (1993) *Water vapour permeability of cement based materials*, report TVBM-1014, Laboratory of Building Materials, Lund University, Lund, http://www.byggnadsmaterial.lth.se/english/publications/#0

Janz, M. (2000) *Moisture transport and fixation in porous materials at high moisture levels*. Report TVB-1018, Laboratory of Building Materials, Lund University, Lund, http://www.byggnadsmaterial.lth.se/english/publications/#0

Johansson, P. (2005) *Water absorption in two-layer masonry systems - properties, profiles and predictions*, report TVBM-1024, Laboratory of Building Materials, Lund University, Lund, http://www.byggnadsmaterial.lth.se/english/publications/#0

van der Kooi, J. (1971) Moisture transport in cellular concrete roofs, Uitgevery Waltman, Delft.

Nilsson, L.-O. (1980) *Hygroscopic moisture in concrete – drying, measurements and related material properties*. Report TVBM-1003, Laboratory of Building Materials, Lund University, Lund

Olsson, N., Baroghel-Bouny, V., Nilsson, L.-O. and Thiery, M. (2012). Non-saturated ion diffusion in concrete – new laboratory measurements. International Congress on Durability of Concrete ICDC 2012, Trondheim.

Radocea, A. (1993) *A study on the mechanism of plastic shrinkage of cement-based materials*. Report P-92:9. Dept. of Building Materials, Chalmers University of Technology, Göteborg

Wadsö, L. (1989). The sorption method – old and new ideas. Report TVBM-3040, Laboratory of Building Materials, Lund University, Lund